Defence Research and Development Canada
Recherche et développement pour la défense Canada

DEFENCE R&D DÉFENSE

A Distributed Drag Force Approach for the Numerical Simulation of Urban Flows

Eugene Yee
Defence R&D Canada – Suffield

Fue-Sang Lien
University of Waterloo

Technical Report
DRDC Suffield TR 2004-169
November 2004

Canada

A Distributed Drag Force Approach for the Numerical Simulation of Urban Flows

Eugene Yee
Defence R&D Canada – Suffield

Fue-Sang Lien
University of Waterloo

Defence R&D Canada – Suffield

Technical Report

DRDC Suffield TR 2004-169

November 2004

Author

Eugene Yee

Approved by

Dr L. Nagata
Head, Chemical and Biological Defence Section

Approved for release by

~~Dr R. Bide~~ P.A. D'Agostino
Chair, DRDC Suffield DRP

Abstract

A modified k-ϵ model is proposed for the simulation of the mean wind speed and turbulence for a neutrally-stratified flow through and over a building array, where groups of buildings in the array are aggregated and treated as a porous barrier. This model is based on time averaging the spatially-averaged Navier-Stokes equation, in which the effects of the obstacle-atmosphere interaction are included through the introduction of a volumetric momentum sink (representing drag on the unresolved buildings in the array). In addition, closure of the time-averaged, spatially-averaged Navier-Stokes equations requires two additional prognostic equations, namely one for the time-averaged sub-filter kinetic energy, $\overline{\kappa}$, and another for the dissipation rate, ϵ, of $\overline{\kappa}$. The transport equation for $\overline{\kappa}$ can be derived from first principles and explicitly includes additional sources and sinks that arise from time averaging the product of the spatially-averaged velocity fluctuations and the distributed drag force fluctuations. The latter time-averaged product can be approximated systematically to any degree of accuracy using a Taylor series expansion and, to this end, a high-order approximation is derived to represent this source/sink term in the transport equation for $\overline{\kappa}$ which corresponds physically to the work done against pressure (form) and viscous drag in the building array. The dissipation rate (ϵ-) equation is simply obtained as a dimensionally consistent analog of the $\overline{\kappa}$-equation.

Because measurements of the spatially-averaged velocity statistics in obstacle arrays are not available, the performance of the proposed model and some simplified versions derived from it are compared with the spatially-averaged, time-mean velocity and various spatially-averaged Reynolds stresses diagnosed from high-resolution computational fluid dynamics (CFD) simulations of the flow within and over an aligned array of sharp-edged cubes with a plan area density of 0.25. However, it should be emphasized that the high-resolution CFD flow simulations have been validated with wind tunnel experiments, and after these validations the model can be used to diagnose the spatially-averaged velocity statistics required for the validation of the distributed drag force model. It was found that the model predictions for mean wind speed and turbulence in the building array were not sensitive to the differing treatments of the source and sink terms in the $\overline{\kappa}$- and ϵ-equations, implying that the high-order approximations of these source/sink terms did not offer any predictive advantage. A possible explanation for this is the utilization of the Boussinesq linear stress-strain constitutive relation within the k-ϵ modelling framework, whose implicit omission of any anisotropic eddy-viscosity effects renders it incapable of predicting any strong anisotropy of the turbulence field that might exist in the building array. Four different methods for diagnosis of the drag coefficient C_D for the aligned cube array, required for the volumetric drag force representation of the cubes, are investigated here.

Résumé

Un modèle modifié k-ε a été proposé pour simuler la vitesse et la turbulence moyennes du vent pour des écoulements d'air de stratification neutre, à travers et par-dessus une matrice de bâtiments. À l'intérieur de la matrice, des groupes de bâtiments ont été agrégés et traités comme une barrière poreuse. Ce modèle est basé sur le calcul des moyennes en temps et en espace de l'équation Navier-Stokes dans lequel les effets de l'interaction entre les obstacles et l'atmosphère sont inclus au moyen de l'introduction d'un accumulateur des impulsions volumétriquese (représentant la traînée sur les bâtiments non résolus dans la matrice). De plus, la fermeture des équations Navier-Stokes, dont les moyennes en temps et espace ont été calculées exigent deux équations de prévision supplémentaires, à savoir, une équation pour l'énergie cinétique sous-filtre $\overline{\kappa}$ dont les moyennes ont été calculées et une autre équation pour le taux de dissipation ε, de $\overline{\kappa}$. L'équation de transport pour $\overline{\kappa}$ peut être dérivée à partir des principes de base et peut inclure explicitement des sources et des puits additionnels provenant du calcul des moyennes en temps du produit des fluctuations des vitesses moyennes en espace et des fluctuations de la force distribuée de traînée. Ce dernier produit aux moyennes calculées peut être évalué systématiquement à n'importe quel niveau d'exactitude en utilisant une expansion de la série de Taylor et, à cet effet, une approximation d'ordre supérieur est dérivée pour représenter ce terme de la source ou de puits dans l'équation de transport pour $\overline{\kappa}$ qui correspond au travail physiquement accompli contre la pression (forme) et la traînée visqueuse, à l'intérieur de la matrice de bâtiments. L'équation du taux de dissipation (ε-) est simplement obtenue comme un analogue de dimension constante de l'équation $\overline{\kappa}$.

La prise de mesures des statistiques de vitesse moyenne en espace n'étant pas possible à l'intérieur des matrices d'obstacles, le rendement du modèle proposé et de celui de quelques versions simplifiées qui en sont dérivées, sont comparés avec la moyenne des vitesses moyennes en espace et de certains efforts de Reynold moyens en espace diagnostiqués à partir de simulations à haute résolution de la dynamique numérique des fluides de l'écoulement à l'intérieur et par-dessus la matrice de cubes à angles vifs alignés d'une masse surfacique de 0,25. Il faut souligner, cependant, que les simulations d'écoulement de la dynamique numérique des fluides à haute résolution ont été validées par des essais dans des tunnels aérodynamiques et qu'après avoir été validé, le modèle peut être utilisé pour diagnostiquer les statistiques de vitesse moyennes en espacerequises pour la validation du modèle de la force distribuée de la traînée. On a trouvé que les prédictions de modèles pour la vitesse et la turbulence moyennes du vent dans la matrice des bâtiments ne sont pas sensibles aux différents traitements des termes de la source et de puits dans les équations $\overline{\kappa}$ - et ε-, ce qui implique que les approximations supérieures des termes de sources de puits n'offrent aucun avantage en ce qui concerne la prédiction. Il est possible d'expliquer ceci par la relation constitutive de la théorie de Boussinesq, à l'intérieur du contexte de modélisation k-ε, dont l'omission implicite des effets anisotropiques de viscosité turbulente le rende incapable de prédire aucune anisotropie forte du champ de la turbulence qui pourrait exister dans la matrice des bâtiments. On étudie ici quatre méthodes différentes de diagnostic du coefficient C_D de la traînée concernant la matrice de cubes alignés requise pour représenter la force de la traînée des cubes.

Executive summary

Introduction: It is anticipated that Canadian Forces (CF) in the foreseeable future will have to fight in or protect urban areas, whether in battle, peace-making, peacekeeping, or counter-terrorist operations. The increased awareness and importance accorded by the public worldwide and their governments to maintain appropriate defences against chemical and biological warfare (CBW) agents in an urban (built-up) environment, the prediction of casualties and human performance degradation resulting from such releases, and the development of operational procedures and regulations to control, mitigate, and monitor the fate of CBW agents in urban areas with high population densities, will require mathematical modeling of urban wind flows and dispersion. In this regard, it should be noted that the prediction of flows in the urban environment is in principle pre-requisite to or co-requisite with the prediction of contaminant (e.g., CBW agent) dispersion within a cityscape.

Results: A modified k-ϵ model is proposed for the simulation of the mean wind speed and turbulence for a neutrally-stratified flow through and over a building array, where groups of buildings in the array are aggregated and treated as a porous barrier. This model is based on time averaging the spatially-averaged Navier-Stokes equation, in which the effects of the obstacle-atmosphere interaction are included through the introduction of a volumetric momentum sink (representing drag on the unresolved buildings in the array). In addition, closure of the time-averaged, spatially-averaged Navier-Stokes equations requires two additional prognostic equations, namely one for the time-averaged sub-filter kinetic energy, $\overline{\kappa}$, and another for the dissipation rate, ϵ, of $\overline{\kappa}$. The transport equation for $\overline{\kappa}$ can be derived from first principles and explicitly includes additional sources and sinks that arise from time averaging the product of the spatially-averaged velocity fluctuations and the distributed drag force fluctuations. The latter time-averaged product can be approximated systematically to any degree of accuracy using a Taylor series expansion and, to this end, a high-order approximation is derived to represent this source/sink term in the transport equation for $\overline{\kappa}$ which corresponds physically to the work done against pressure (form) and viscous drag in the building array. The dissipation rate (ϵ-) equation is simply obtained as a dimensionally consistent analog of the $\overline{\kappa}$-equation.

The performance of the proposed model and some simplified versions derived from it are compared with the spatially-averaged, time-mean velocity and various spatially-averaged Reynolds stresses diagnosed from high-resolution computational fluid dynamics (CFD) simulations of the flow within and over an aligned array of sharp-edged cubes with a plan area density of 0.25. It was found that the model predictions for mean wind speed and turbulence in the building array were not sensitive to the differing treatments of the source and sink terms in the $\overline{\kappa}$- and ϵ-equations, implying that the high-order approximations of these source/sink terms did not offer any predictive advantage. A possible explanation for this is the utilization of the Boussinesq linear stress-strain constitutive relation within the k-ϵ modelling framework, whose implicit omission of any anisotropic eddy-viscosity effects renders it incapable of predicting any strong anisotropy of the turbulence field that might exist in the building array. Four different methods for diagnosis of the drag coefficient C_D for the aligned cube array, required for the volumetric drag force representation of the cubes, are investigated here.

Significance and Future Plans: A knowledge of the structure of the mean flow and turbulence describing the complex flow patterns within and over clusters of buildings is essential for improving urban dispersion models. Unfortunately, the computational demands of computational fluid dynamics (CFD) where all buildings are resolved explicitly in the sense that boundary conditions are imposed at all surfaces (e.g., walls, roofs) are so prohibitive as to preclude their use for emergency response situations which require the ability to generate an urban flow and dispersion prediction in a time frame that will permit protective actions to be taken. In view of this, we have demonstrated in this report how to construct models for the statistics of the mean flow and turbulence in an urban canopy that are obtained by averaging horizontally the mean wind and turbulence statistics over an area that is larger than the spacings between the individual roughness elements comprising the urban canopy, but less than the length scales over which the roughness element density changes. The development of spatially-averaged Reynolds-averaged Navier-Stokes models permits an efficient prediction of urban flows required for emergency response situations. The utility of the simplified urban flow simulation models investigated here for provision of the disturbed wind field statistics required by a physically-based dispersion model needs further investigation.

Yee, E. and Lien, F.S. (2004). A Distributed Drag Force Approach for the Numerical Simulation of Urban Flows. (DRDC Suffield TR 2004-169). Defence R&D Canada – Suffield.

Sommaire

Introduction : On prévoit que les Forces canadiennes (FC), auront, dans un avenir assez rapproché, à combattre à l'intérieur de zones urbaines ou à protéger ces dernières, durant des opérations de combat, de maintien de la paix ou antiterroristes. Une prise de conscience accrue et l'importance que le monde entier et ses gouvernements accordent au maintien de moyens de défense appropriés contre les agents de guerre chimiques et biologiques (CB) dans les milieux urbains (construits), à la prévision des blessés et la dégradation de la performance humaine résultant de telles émissions ainsi qu'à la mise au point de procédures opérationnelles et de règlements de contrôle pour atténuer et surveiller le sort des agents CB dans les zones urbaines comprenant des hautes densités de population, exigeront des modélisations mathématiques des écoulements éoliens urbains et de leur dispersion. À cet égard, il faut noter que la prévision des écoulements dans un milieu urbain est en principe pré-requise ou co-requise avec la prévision de la dispersion du contaminant (par ex. : agent CB), dans un paysage urbain.

Résultats : Un modèle modifié k-ε a été proposé pour simuler la vitesse et la turbulence moyennes du vent pour des écoulements d'air de stratification neutre, à travers et par-dessus une matrice de bâtiments. À l'intérieur de la matrice, des groupes de bâtiments ont été agrégés et traités comme une barrière poreuse. Ce modèle est basé sur le calcul des moyennes en temps et en espace de l'équation Navier-Stokes, dans lequel les effets de l'interaction entre les obstacles et l'atmosphère sont inclus au moyen de l'introduction d'un accumulateur des impulsions volumétriques (représentant la traînée sur les bâtiments non résolus dans la matrice). De plus, la fermeture des équations Navier-Stokes, dont les moyennes en temps et en espace ont été calculées, exigent deux équations de prévision supplémentaires, à savoir, une équation pour l'énergie cinétique sous-filtre $\overline{\kappa}$ dont les moyennes ont été calculées et une autre équation pour le taux de dissipation ε, de $\overline{\kappa}$. L'équation de transport pour $\overline{\kappa}$ peut être dérivée à partir des premiers principes et peut inclure explicitement des sources et des puits additionnels provenant du calcul des moyennes en temps du produit des fluctuations des vitesses moyennes en espace et des fluctuations de la force distribuée de traînée. Ce dernier produit aux moyennes calculées peut être évalué systématiquement à n'importe quel niveau d'exactitude en utilisant une expansion de la série de Taylor et, à cet effet, une approximation d'ordre supérieur est dérivée pour représenter ce terme de la source ou de piégeage dans l'équation de transport pour $\overline{\kappa}$ qui correspond au travail physiquement accompli contre la pression (forme) et la traînée visqueuse, à l'intérieur de la matrice de bâtiments. L'équation du taux de dissipation (ε-) est obtenue simplement comme un analogue de dimension constante de l'équation $\overline{\kappa}$.

Le rendement du modèle proposé et de quelques versions simplifiées qui en sont dérivées, sont comparés entre la moyenne des vitesses instantanées, dont les moyennes en espace ont été calculées et des tensions de Reynold variées dont les moyennes en espace ont été calculées, diagnostiquées à partir de simulations à haute résolution de la dynamique numérique des fluides de l'écoulement à l'intérieur et par-dessus la matrice de cubes à angles vifs alignés d'une masse surfacique de 0,25. On a trouvé que les prédictions de modèles pour la vitesse et la turbulence moyennes du vent dans la matrice des bâtiments ne sont pas sensibles aux différents traitements des termes de la source et de puits dans les équations $\overline{\kappa}$ -

et ε-, ce qui implique que les approximations supérieures des termes de sources /de puits n'offrent aucun avantage en ce qui concerne la prédiction. Il est possible d'expliquer ceci par la relation constitutive de la théorie de Boussinesq, à l'intérieur du contexte de modélisation k-ε, dont l'omission implicite des effets anisotropiques de viscosité turbulente le rende incapable de prédire aucune anisotropie forte du champ de la turbulence qui pourrait exister dans la matrice des bâtiments. On étudie ici quatre méthodes différentes de diagnostic du coefficient C_D de la traînée pour la matrice de cubes alignés qui est requise pour représenter la force de la traînée des cubes.

La portée des résultats et les plans futurs : Il est essentiel de connaître la structure de l'écoulement moyen et de la turbulence moyenne qui décrit les modèles complexes d'écoulement à l'intérieur et par-dessus des réseaux de bâtiments et qui vise à améliorer les modèles urbains de dispersion. Malheureusement, tous les bâtiments étant résolus explicitement avec des conditions de limites imposées sur toutes les surfaces (par ex. : murs, toits), les exigences en calculs de la dynamique numérique des fluides rendent impossible l'utilisation de cette méthode en cas d'une intervention d'urgence ; une situation d'intervention d'urgence exige de générer une prédiction des écoulements et de la dispersion en milieu urbain dans un délai d'exécution assez bref pour permettre la prise des mesures de protection. Dans cette optique, nous avons démontré dans ce rapport, comment construire des modèles de statistiques concernant l'écoulement moyen et les turbulences moyennes dans une couverture urbaine. Ces modèles sont obtenus en calculant la moyenne horizontale des statistiques de l'écoulement moyen et des turbulences moyennes du vent, sur un territoire plus large que l'espacement entre les éléments individuels de rugosité comprenant la couverture urbaine mais moins large que les échelles de longueur couvrant un territoire sur lequel change la densité de l'élément de rugosité. La mise au point des modèles Reynold et Navier-Stokes, dont les moyennes en espace ont été calculées, permet une prédiction efficace des écoulements urbains pour des situations d'intervention d'urgence. L'utilité des modèles simplifiés de simulation de l'écoulement urbain ayant été étudiée ici pour les statistiques de champs de vent perturbé requis par le modèle de dispersion, d'après des critères physiques, exige d'être étudiée plus profondément.

Yee, E. and Lien, F.S. (2004). A Distributed Drag Force Approach for the Numerical Simulation of Urban Flows. (DRDC Suffield TR 2004-169). R & D pour la défense Canada – Suffield.

Table of contents

List of Figures

This page left intentionally blank.

Introduction

The turbulent flow within and over urban areas covered with agglomerations of discrete buildings, often with irregular geometry and spacing, is generally very complex and possesses a fully three-dimensional structure. Although the application of computational fluid dynamics (CFD) to the prediction of the mean flow and turbulence near and around a single building or within and over a regular array (or, canopy) of buildings is progressing ([1], [2], [3], [4]), this method tends to require extensive computational resources. Nevertheless, CFD simulations which involve the solution of the conservation equations for mass, momentum, and energy allow the prognosis of a number of velocity statistics (e.g., mean velocity, normal stresses, shear stresses, etc.) in an urban canopy. A knowledge of the structure of the mean flow and turbulence describing the complex flow patterns within and over clusters of buildings is also essential for improving urban dispersion models.

Unfortunately, the computational demands of CFD where all buildings are resolved explicitly in the sense that boundary conditions are imposed at all surfaces (e.g., walls, roofs) are so prohibitive as to preclude their use for emergency response situations which require the ability to generate an urban flow and dispersion prediction in a time frame that will permit protective actions to be taken. In view of this, we argue that for many practical applications it is convenient to consider the prediction of spatial averages of the mean wind and turbulence in an urban canopy that is obtained by averaging horizontally the mean wind and turbulence statistics over an area that is larger than the spacings between the individual roughness elements comprising the urban canopy, but less than the length scale over which the roughness element density changes.

In this report, we focus on the mathematical formulation of a numerical model for the prediction of flows within and over a building array based on an aggregation of groups of buildings in the array into a number of 'drag units', with the ensemble of units being treated as a continuous porous medium. This approach will obviate the need to impose boundary conditions along the surfaces of all buildings (and other obstacles) in the array. Wilson and Yee [5] applied something like this approach to simulate the mean wind and turbulence energy fields in a single unit cell of the wind tunnel "Tombstone Canopy" [6], a regular diamond staggered array of bluff (impermeable) aluminum plates, with a disappointing outcome (subsequent work showed that invoking a Reynolds stress closure did not help). We now know this may owe to the existence of (previously unsuspected) large eddies generated by the strong shear layer near the top of the canopy, eddies that span more than one unit cell in the streamwise direction, and imply that imposition of an artificial condition of periodicity at the boundaries of a single cell amounts to solving a different flow problem. These large-scale (coherent) eddy structures generated at or near the canopy top have been observed using highly resolved, two-dimensional laser-induced fluorescence measurements of the fine structure of the fully space- and time-varying conserved scalar field resulting from a point-source release of a tracer within the "Tombstone Reloaded Canopy" in a water channel simulation [7]. Belcher et al. [8] applied a similar approach to investigate the adjustment of the mean velocity to a canopy of roughness elements using a linearized flow model (obtained by determining analytically small perturbations to the undisturbed upstream logarithmic mean velocity profile induced by the drag due to an obstacle array). Hookham et al. [9] have used a drag force parameterization to represent the effects of buildings on the flow in the development of their Urban Windfield Module.

There is precedent for treating drag on unresolved buildings in an urban canopy by means of a distributed momentum sink for the representation of the effects on the mean flow and turbulence arising from the form and viscous drag on canopy elements. As motivation, we recall that a similar approach has been applied over the past 50 years to the modelling of flows in plant canopies and about porous windbreaks. Although a sink or drag term has been added in an *ad hoc* fashion to the free-air mean momentum equation to model the canopy mean wind profile over a number of years ([10], [11], [12]), it was not until 1977 that Wilson and Shaw [13] showed how to apply a rigorous spatial-averaging procedure to obtain the equations for a spatially-continuous area-averaged mean wind and turbulence field. In this seminal work, Wilson and Shaw [13] demonstrated how additional source and sink terms representing the flow interaction with the canopy elements emerge naturally by application of a particular spatial averaging procedure to the Reynolds-averaged Navier-Stokes equations that obtain at every point in the canopy airspace. This procedure was further developed by Raupach and Shaw [14] for the case of a horizontal plane averaging operation. In particular, Raupach and Shaw [14] discuss two different options for averaging over a horizontal plane; namely, horizontally averaging the equations of motion at a single time instant over a plane extensive enough "to eliminate variations due to canopy structure and the largest length scales of the turbulent flow" (scheme I) and conventional time averaging of the equations of motion followed by horizontal averaging over a plane large enough "to eliminate variations in the canopy structure" (scheme II). Scheme I has rather limited applicability since it cannot be applied to horizontally inhomogeneous canopies.

Finnigan [15] and Raupach et al. [6] investigated the volume-averaging method. Finnigan [15] considered details such as plant motion (e.g., coherently waving plant canopies) which gives rise to a 'waving production' term in the transport equations for turbulence quantities. We note that plant motion is not a factor directly pertinent to the present work which focusses on urban canopy flows, but these concepts may have a bearing on the case of moving obstacles (e.g., vehicles) within the urban canopy. Following ideas of Hanjalic et al. [16] and parallelling Shaw and Seginer [17], Wilson [18] developed an empirical two-band model for the turbulence kinetic energy (TKE) which represented the large- and fine-scale components of the turbulence and their dynamics [the multiple time-scale approach has seen much subsequent use [19], but parameterizing the exchange of kinetic energy between the spectral bands is a pre-eminent difficulty of the approach]. Here, the turbulence kinetic energy was separated into two wave-bands, corresponding to shear kinetic energy (SKE, low-frequency band) and wake kinetic energy (WKE, high-frequency band), with separate equations developed to represent their dynamics. Wilson [20], Green [21], Wang and Takle [22], Wang and Takle [23], Liu et al. [24], Ayotte et al. [25], Sanz [26], and Wilson and Yee [27] investigated various modifications of the k-ϵ model or the Reynolds stress transport model to account for interaction of the air with canopy elements.

This is the final report of two describing the numerical modelling of the developing flow within and over a 3-D building array. In the first report (henceforth I) [4], we used the Reynolds-averaged Navier-Stokes (RANS) equations in conjunction with a two-equation turbulence model (i.e., k-ϵ model) to predict the complex three-dimensional disturbed flow within and over a 3-D building array under neutral stability conditions. The simulations of the mean flow field and turbulence kinetic energy were validated with data obtained from a comprehensive wind tunnel experiment conducted by Brown et al. [28]. Here, it was demonstrated that the mean flow and turbulence kinetic energy from the numerical and physical simulations exhibited striking resemblences. In addition, the importance of the

kinematic 'dispersive stresses' relative to the spatially-averaged kinematic Reynolds stresses for developing flow within and over an urban-like roughness array has been quantified using the high-resolution CFD results obtained with the high-Reynolds-number k-ϵ model.

In this report, we focus on the formulation of a numerical model for the prediction of flows within and over a building array based on an aggregation of groups of buildings in the array into a number of 'drag units', with each unit being treated as a porous barrier. This approach will obviate the need to impose boundary conditions along the surfaces of all buildings (and other obstacles) in the array. Here, we present details of the mathematical framework required to derive the transport equation for the time average of the locally-spatially-averaged velocity through a building array (which is treated here as a porous medium), and the two additional prognostic equations required to close this equation set. These additional equations predict the time-averaged resolved-scale kinetic energy of turbulence, $\overline{\kappa}$, and its dissipation rate, ϵ. The closure problem relating to the 'correct' representation of the additional source/sink terms in the transport equations for mean momentum, turbulence energy, and dissipation rate is investigated in detail. Most of the work reported is motivated by conceptual and logical difficulties in the self-consistent treatment of source and sink terms in the transport equations for turbulence kinetic energy and its dissipation rate. To this end, we attempt to lay the foundations for a systematic mathematical formulation that could be used to construct the additional source/sink terms in the transport equations for $\overline{\kappa}$ and ϵ, in response (and to some extent, contradiction) to the assertions made by Wilson and Mooney [29] that it is "impossible to know the 'correct' influence of the unresolved processes at the fence on TKE and its dissipation rate" and by Wilson et al. [30] that "k-ϵ closures give predictions that are sensitive to details of ambiguous choices". The problem of the diagnosis of the drag coefficient C_D required in the parameterization of the distributed drag is addressed. We show detailed comparisons of predictions obtained from the model with spatial averages of the mean velocity field and second-order velocity statistics obtained from a high-resolution CFD simulation of flow within and over a 3-D building array.

Model formulation

Spatial and time averaging operations

Before we begin, we present a short note on the notation that will be used. The following derivations will invariably use the flexibility of the Cartesian tensor notation, with Roman indices such as i, j, or k taking values of 1, 2, or 3. We shall also employ the Einstein summation convention in which repeated indices are summed. For any flow variable ϕ, $\langle\phi\rangle$ will denote the spatial (volume) average, $\overline{\phi}$ the time average, ϕ' the departure of ϕ from its time-averaged value, and ϕ'' the departure of ϕ from its spatially-averaged value. In addition, u_i is the total velocity in the x_i-direction, with $i = 1$, 2, or 3 representing the streamwise x, spanwise y, or vertical z direction. Finally, $\mathbf{x} \equiv (x, y, z)$, $(u_1, u_2, u_3) \equiv (u, v, w)$, and t denotes time.

The derivation of a model for the spatially-averaged time-mean flow can start either from applying the spatial averaging operation to the time-averaged Navier-Stokes (NS) equation ($\langle\overline{\mathrm{NS}}\rangle$), or the time averaging operation to the spatially-averaged Navier-Stokes equation ($\overline{\langle\mathrm{NS}\rangle}$). In formulating such equations, we must choose a suitable decomposition of a

flow property into its rapidly and slowly varying components and determine a strategy for applying the corresponding averaging operation. First, consider spatial averaging in some multiply connected space. In a "slow + fast" decomposition of a flow property ϕ based on spatial filtering, scales are separated by applying a low-pass scale filter to give a filtered quantity $\langle\phi\rangle$ defined by

$$\langle\phi\rangle(\mathbf{x}) = \int_{\text{a.s.}} G(\mathbf{x}-\mathbf{y})\phi(\mathbf{y})\,d\mathbf{y} \equiv G\star\phi. \tag{1}$$

The integral in Equation (1) is assumed to be over all space (a.s.). Here, $G(\mathbf{x}-\mathbf{y})$, the convolution filter kernel, is a localized function (i.e., $G \to 0$ as $\|\mathbf{x}-\mathbf{y}\| \to \infty$, where $\|\cdot\|$ denotes the Euclidean norm) with width Δ which is related to some cutoff scale in space, and $\star$ is used to denote the convolution operation. In general, the filter width can depend on $\mathbf{x}$, which we will explicitly indicate using the notation $G\big(\mathbf{x}-\mathbf{y}\big|\Delta(\mathbf{x})\big)$.

If we assume that G is a symmetric function of $\mathbf{x}-\mathbf{y}$, and differentiate Equation (1) with respect to x_i, we get the following relationship between the spatial average of the spatial derivative and the spatial derivative of the spatial average of a quantity ϕ (on application of the Gauss divergence theorem):

$$\begin{aligned}\left\langle\frac{\partial\phi}{\partial x_i}\right\rangle - \frac{\partial\langle\phi\rangle}{\partial x_i} &\equiv \left[G\star, \frac{\partial}{\partial x_i}\right]\phi \\ &= -\left(\frac{\partial G}{\partial\Delta}\star\phi\right)\frac{\partial\Delta}{\partial x_i} \\ &\quad + \int_S G\big(\mathbf{x}-\mathbf{y}\big|\Delta(\mathbf{x})\big)\phi(\mathbf{y})n_i\,dS,\end{aligned} \tag{2}$$

where S denotes the sum of all obstacle surfaces contained in the multiply connected region (extending over all space), n_i is the unit outward normal in the i-th direction on the surface S (positive when directed into the obstacle surface), and $[f,g] \equiv fg - gf$ denotes the commutator bracket of two operators f and g. Equation (2) will be referred to as the generalized spatial averaging theorem. A special case of this theorem (known as the spatial averaging theorem) has been derived by Raupach and Shaw [14] and Howes and Whitaker [31].

The spatial filtering operation does not commute with spatial differentiation. The non-commutation of these two operations results from two contributions. The first contribution is encapsulated in the first term on the right-hand-side of Equation (2) which arises from the spatial variation in filter cutoff length. The second contribution, summarized in the second term on the right-hand-side of Equation (2), is due to the presence of obstacle surfaces in the multiply connected flow domain. Interestingly, if we apply the spatial-averaging operator to the continuity equation, the spatial variation in the filter width implies that $\langle u_i\rangle$ is no longer solenoidal. More specifically, although the velocity across the air/solid boundaries vanishes owing to the no-slip and impermeability boundary conditions here, the spatial variation of the filter width implies an extra source/sink term in the filtered continuity equation [which is a direct consequence of Equation (2)]:

$$\frac{\partial\langle u_i\rangle}{\partial x_i} = -\left[G\star, \frac{\partial}{\partial x_i}\right]u_i = \left(\frac{\partial G}{\partial\Delta}\star u_i\right)\frac{\partial\Delta}{\partial x_i}. \tag{3}$$

To ensure that the spatially-averaged velocity field is solenoidal, we consider a special convolution kernel whose filter cutoff length does not depend on $\mathbf{x}$. To this purpose, consider the box or top-hat filter defined as

$$G(\mathbf{x}-\mathbf{y}) = \begin{cases} 1/V, & \text{if } |x_i - y_i| \le \Delta_i/2; \\ 0, & \text{otherwise.} \end{cases} \tag{4}$$

Here, $V = \Delta_x \Delta_y \Delta_z$ is the *constant* volume over which we average to obtain continuous variables. With the constant width filter kernel of Equation (4), the spatial average of a flow property ϕ of Equation (1) becomes simply

$$\langle \phi \rangle(\mathbf{x}, t) = \frac{1}{V} \int_V \phi \, dV \equiv \frac{1}{V} \int_V \phi(\mathbf{x} + \mathbf{r}, t) \, d\mathbf{r}. \tag{5}$$

Note that in Equation (5), the averaging volume includes *both* fluid and solid parts (obstacles). Applying the volume-averaging operator of Equation (5) to the continuity equation results in a spatially-averaged velocity field $\langle u_i \rangle$ that is solenoidal.

We will use the spatial-averaging operation displayed in Equation (5), where the average is taken over both the fluid and solid phases in V (averaging volume), and the normalizing factor is the total volume V. For two-phase systems, two other definitions for averaging have been proposed (e.g., Miguel et al.[32]). In a two-phase system, the total averaging volume V is made up of the volume of the fluid phase V_f and the solid phase V_s, so $V = V_f + V_s$. The superficial (external) phase average of ϕ is defined as

$$\langle \phi \rangle_e = \frac{1}{V} \int_{V_f} \phi \, dV \tag{6}$$

and the intrinsic (internal) phase average of ϕ is defined as

$$\langle \phi \rangle_i = \frac{1}{V_f} \int_{V_f} \phi \, dV. \tag{7}$$

The intrinsic phase average is an average of a flow property over the fluid phase (i.e., the averaging volume V_f excludes the solid phase, with the normalizing factor being V_f). On the other hand, the external phase average is a weighted average of the fluid property over the fluid phase (i.e., the total volume V is used as the normalizing factor, but the averaging excludes the solid phase).

The spatial (or, volume) average defined in Equation (5) seems natural in the present context, and leads to the simplest forms for the volume-averaged transport equations on application of the volume-averaging operator to the continuity and the Reynolds equation for mean momentum at a single point. Although V is a constant that is independent of the spatial coordinates, V_f which represents the volume of the fluid phase contained within V need not be (e.g., for an inhomogeneous canopy, V_f and V_s will be a function of the spatial coordinates). Because V_f depends on $\mathbf{x}$ in Equation (7) (i.e., the filter width depends on $\mathbf{x}$), the use of the intrinsic phase average will result in a filtered velocity that is not solenoidal [cf. Equation (3)]. Even so, transport equations for the intrinsic phase-averaged velocity $\langle u_j \rangle_i$ can be derived, provided that the fluid-phase volume $V_f(\mathbf{x})$ is differentiable (or, equivalently, that the porosity $\xi \equiv V_f/V$ is a differentiable function of $\mathbf{x}$) although this

will result in a number of 'extra' source/sink terms in these equations arising solely from the dependence of V_f on the spatial coordinates. The external phase average does not seem natural in the present context because $\langle\langle\phi\rangle_e\rangle_e \neq \langle\phi\rangle_e$[1] (or, equivalently, $\langle\phi_e''\rangle_e \neq 0$ where $\phi_e'' \equiv \phi - \langle\phi\rangle_e$).

In analogy with the spatial (or, volume) average defined in Equation (5), the time average of ϕ, which we denote using an overbar, will be defined as

$$\bar{\phi}(\mathbf{x}) = \frac{1}{T}\int_{t_0}^{t_0+T} \phi(\mathbf{x},t)\,dt, \qquad T_1 \ll T \ll T_2. \tag{8}$$

In view of Equations (5) and (8), time and spatial averaging commute so $\overline{\langle\phi\rangle} = \langle\bar{\phi}\rangle$. In Equation (5), the horizontal averaging scales Δ_x, Δ_y need to be large compared to the separation between individual roughness elements, but much less than the characteristic length scales over which the density of the roughness elements changes; but to ensure a sufficient vertical resolution of the flow property gradients, $\Delta_z \ll \Delta_x, \Delta_y$ making V a thin, horizontal slab. In Equation (8), the averaging time T is implicitly assumed to be sufficiently long to ensure that many cycles of the rapid turbulent fluctuations in a flow property are captured, but sufficiently short so that the external large-scale variations in the flow property are approximately constant. Hence, in Equation (8), T_1 and T_2 denote the time scales characteristic of the rapid and slow variations in the flow property ϕ, with the implicit assumption that T_1 and T_2 differ by several orders of magnitude.

In general, ϕ can be decomposed in the following two ways:

$$\phi = \bar{\phi} + \phi', \qquad \overline{\phi'} = 0, \tag{9}$$

or

$$\phi = \langle\phi\rangle + \phi'', \qquad \langle\phi''\rangle = 0. \tag{10}$$

Although $\langle\overline{\mathrm{NS}}\rangle = \overline{\langle\mathrm{NS}\rangle}$ owing to the commutation of time and spatial averaging operations, space-time filtering and time-space filtering of the Navier-Stokes equation lead to two different decompositions for the turbulent stress tensor, a quantity that needs to be modelled (viz., the turbulence closure problem). The subtle differences in these two decompositions for the turbulent stress tensor (arising from either a space-time or time-space filtering of the nonlinear convective term in the Navier-Stokes equation) will be elucidated in the following subsections.

Spatial average of the time-averaged NS equation

The spatial average of the time-averaged NS equation (or spatial average of the RANS equation) has been described in detail by Raupach and Shaw [14], Ayotte et al. [25], and others. Consequently, only some final results are summarized here for later reference. The spatially-averaged RANS equation for the prediction of the spatially-averaged time-mean velocity $\langle\overline{u_i}\rangle$ is

$$\frac{\partial\langle\bar{u}_j\rangle\langle\bar{u}_i\rangle}{\partial x_j} = -\frac{\partial\langle\bar{p}\rangle}{\partial x_i} + \frac{\partial}{\partial x_j}(\tau_{ij}) + \bar{f}_i, \tag{11}$$

[1] Note that after spatial averaging, a flow property ϕ is a continuous function of the coordinates in a multiply connected space. Hence, even though ϕ may vanish identically in the solid phase within V, its spatially-averaged value $\langle\phi\rangle_e$ is continuous and nonzero in V, so $\langle\langle\phi\rangle_e\rangle_e \neq \langle\phi\rangle_e$.

with

$$\tau_{ij} = -\overline{\langle u_i' u_j' \rangle} - \langle \bar{u}_i'' \bar{u}_j'' \rangle + \nu \frac{\partial \langle \bar{u}_i \rangle}{\partial x_j}, \tag{12}$$

and

$$\bar{f}_i = \underbrace{\frac{\nu}{V} \int_S \frac{\partial \bar{u}_i}{\partial n} dS}_{\text{viscousdrag}} - \underbrace{\frac{1}{V} \int_S \bar{p} n_i dS}_{\text{formdrag}}. \tag{13}$$

Here, $\bar{p}$ is the kinematic mean pressure, $\bar{f}_i$ is the total mean drag force per unit mass of air in the averaging volume composed of the sum of a form (pressure) drag and a viscous drag, and τ_{ij} is the spatially-averaged kinematic total stress tensor. In Equation (13), ν is the kinematic viscosity, S is the part of the bounding surface in the averaging volume V that coincides with the obstacle surfaces, n_i is a unit normal vector in the ith direction pointing from V into S (viz., directed from the fluid into the solid surface), and $\partial/\partial n$ denotes differentiation along n_j. Note that the spatially-averaged kinematic Reynolds stresses $\overline{\langle u_i' u_j' \rangle}$ and kinematic dispersive stresses $\langle \bar{u}_i'' \bar{u}_j'' \rangle$ are a direct consequence of the spatial averaging of the time-averaged nonlinear convective term $u_i u_j$; viz.,

$$\overline{\langle u_i u_j \rangle} = \langle \bar{u}_i \rangle \langle \bar{u}_j \rangle + \overline{\langle u_i' u_j' \rangle} + \langle \bar{u}_i'' \bar{u}_j'' \rangle. \tag{14}$$

The last term on the right-hand-side of Equation (14) is the dispersive stress which arises from the spatial correlation in the time-mean velocity field varying with position in the averaging volume V. Although Ayotte et al. [25] rigorously derive the transport equation for $\overline{\langle u_i' u_j' \rangle}$, the extra source/sink terms in their proposed model for the spatially-averaged second central velocity moments $\overline{u_i' u_j'}$, which they denote as d_{ij} (contribution to the total dissipation arising from the canopy interaction processes), were obtained from an approximate expression for the work done by the fluctuating turbulence against the fluctuating drag force. The latter was derived in the context of the time average of the spatially-averaged NS equation. Mixing the spatially-averaged RANS formulation with the time-averaged, spatially-averaged NS formulation results in a mathematical inconsistency in the approach described by Ayotte et al. [25].

In the next subsection, we formulate the equation set for the time-averaged, spatially-averaged NS approach. The approach taken here is similar to that proposed by Wang and Takle [22] and Getachew et al. [33].

Time average of spatially-averaged NS equation

The spatial average of the nonlinear convective term $u_i u_j$ in the Navier-Stokes equation can be expanded as follows:

$$\langle u_i u_j \rangle = \left\langle \left(\langle u_i \rangle + u_i'' \right) \left(\langle u_j \rangle + u_j'' \right) \right\rangle = \langle u_i \rangle \langle u_j \rangle + \langle u_i'' u_j'' \rangle. \tag{15}$$

Using the decomposition for the spatially-averaged nonlinear convective term of Equation (15), and applying the spatial averaging theorem in Equation (2) with the filter kernel defined in Equation (4), the spatially-averaged NS equation assumes the form

$$\frac{\partial \langle u_j \rangle \langle u_i \rangle}{\partial x_j} = -\frac{\partial \langle p \rangle}{\partial x_i} + \frac{\partial}{\partial x_j}(T_{ij}) + f_i, \tag{16}$$

where

$$T_{ij} = -\langle u_i'' u_j'' \rangle + \nu \frac{\partial \langle u_i \rangle}{\partial x_j}, \tag{17}$$

and

$$f_i = \frac{\nu}{V} \int_S \frac{\partial u_i}{\partial n} \, dS - \frac{1}{V} \int_S p n_i dS. \tag{18}$$

Time-averaging Equation (16) gives the time-averaged, spatially-averaged Navier-Stokes equation $\overline{\langle \mathrm{NS} \rangle}$ as

$$\frac{\partial \langle \bar{u}_j \rangle \langle \bar{u}_i \rangle}{\partial x_j} = -\frac{\partial \langle \bar{p} \rangle}{\partial x_i} + \frac{\partial}{\partial x_j}(\tau_{ij}) + \bar{f}_i, \tag{19}$$

where

$$\tau_{ij} \equiv -\overline{\langle u_i' \rangle \langle u_j' \rangle} + \overline{T_{ij}} = -\overline{\langle u_i' \rangle \langle u_j' \rangle} - \overline{\langle u_i'' u_j'' \rangle} + \nu \frac{\partial \langle \bar{u}_i \rangle}{\partial x_j}, \tag{20}$$

and $\bar{f}_i$ here is the same as $\bar{f}_i$ defined in Equation (13).

From Equations (11), (12), (19) and (20), the following relationship holds:

$$\overline{\langle u_i' u_j' \rangle} + \langle \bar{u}_i'' \bar{u}_j'' \rangle = \overline{\langle u_i' \rangle \langle u_j' \rangle} + \overline{\langle u_i'' u_j'' \rangle}. \tag{21}$$

Equation (21) is the necessary and sufficient condition for $\langle \overline{\mathrm{NS}} \rangle = \overline{\langle \mathrm{NS} \rangle}$. The total stress tensors τ_{ij}, defined in either Equation (12) or Equation (20) are identical (hence, the same notation is used for these two quantities), although the individual terms in their sums are different. We note that the physical character of the term $\overline{\langle u_i'' u_j'' \rangle}$ is different from the conventional dispersive term $\langle \bar{u}_i'' \bar{u}_j'' \rangle$.

From the turbulence modelling point of view, we will model $\overline{\langle u_i' \rangle \langle u_j' \rangle}$ in Equation (20) using the Boussinesq eddy viscosity (ν_t) closure as follows:

$$\overline{\langle u_i' \rangle \langle u_j' \rangle} = \frac{2}{3} \delta_{ij} \overline{\kappa} - \nu_t \left(\frac{\partial \langle \bar{u}_i \rangle}{\partial x_j} + \frac{\partial \langle \bar{u}_j \rangle}{\partial x_i} \right). \tag{22}$$

Here $\overline{\kappa}$ and ν_t are defined as

$$\overline{\kappa} \equiv \frac{1}{2} \overline{\langle u_i' \rangle \langle u_i' \rangle}, \qquad \nu_t = C_\mu \frac{\overline{\kappa}^2}{\epsilon}, \tag{23}$$

and ϵ is defined as

$$\epsilon \equiv \nu \overline{\frac{\partial \langle u_i' \rangle}{\partial x_k} \frac{\partial \langle u_i' \rangle}{\partial x_k}}. \tag{24}$$

In Equation (23), C_μ is a closure (empirical) constant taken to be 0.09 as in the standard k-ϵ model for turbulence closure [34]. We note that κ is the sub-filter kinetic energy, so $\overline{\kappa}$ is the time-averaged sub-filter kinetic energy. In addition, since the filter in Equation (5) is positive (volume averaging), κ is necessarily a positive semi-definite quantity.

To make further progress, we assume

$$\overline{\langle u_i'' u_j'' \rangle} \ll \overline{\langle u_i' \rangle \langle u_j' \rangle} \tag{25}$$

in the present study (viz., we will simply neglect the term $\overline{\langle u_i'' u_j'' \rangle}$ for expediency since no reference data exists at this time to guide its modelling). Before we derive the model equations for $\overline{\kappa}$ and ϵ, let us examine the momentum sink f_i (arising from the pressure and viscous forces created by the obstacle elements in V) in the spatially-averaged NS equation [cf. Equations (16) and (18)]. The drag force term will be parameterized using the following common formulation

$$f_i = -C_D \hat{A} \big(\langle u_j \rangle \langle u_j \rangle \big)^{1/2} \langle u_i \rangle, \tag{26}$$

where C_D is the element drag coefficient and $\hat{A}$ is the frontal area density (frontal area of obstacles exposed to the wind per unit volume). Equation (26) can be interpreted simply as a definition for C_D. Although the drag coefficient is almost invariably assumed to be a constant for a particular canopy, it will be shown later that C_D is a function of position (x, z) within the canopy.

Following from this parameterization, $\bar{f}_i$ (time-averaged momentum sink) in Equation (13) is required to be modelled (approximated) as

$$\bar{f}_i = -C_D \hat{A} \overline{\big(\langle u_j \rangle \langle u_j \rangle \big)^{1/2} \langle u_i \rangle}. \tag{27}$$

Substituting $\langle u_i \rangle = \langle \bar{u}_i \rangle + \langle u_i' \rangle$ into Equation (26) and using the binomial theorem to approximate the square root term (see also Getachew et al. [33]), an approximate form for f_i that is appropriate for time averaging can be derived as

$$\begin{aligned} f_i \approx -C_D \hat{A} Q \Bigg(& \langle \bar{u}_i \rangle + \frac{\langle \bar{u}_i \rangle \langle \bar{u}_j \rangle \langle u_j' \rangle}{Q^2} + \langle u_i' \rangle \\ & + \frac{\langle u_i' \rangle \langle \bar{u}_j \rangle \langle u_j' \rangle}{Q^2} + \frac{\langle \bar{u}_i \rangle \langle u_j' \rangle \langle u_j' \rangle}{2Q^2} \Bigg), \end{aligned} \tag{28}$$

where $Q \equiv \big(\langle \bar{u}_i \rangle \langle \bar{u}_i \rangle \big)^{1/2}$ is the magnitude of the spatially-averaged, time-mean wind speed.

Time averaging of f_i in Equation (28) gives the following expression (approximation) for the time-averaged form and viscous drag force vector exerted on a unit mass of air in the averaging volume:

$$\bar{f}_i = -C_D \hat{A} \left(Q \langle \bar{u}_i \rangle + \frac{\langle \bar{u}_j \rangle}{Q} \overline{\langle u_i' \rangle \langle u_j' \rangle} + \frac{\langle \bar{u}_i \rangle \overline{\kappa}}{Q} \right), \tag{29}$$

which, in combination with Equation (22), yields

$$\bar{f}_i = -C_D \hat{A} \left[\left(Q + \frac{5}{3} \frac{\overline{\kappa}}{Q} \right) \langle \bar{u}_i \rangle - \nu_t \left(\frac{\partial \langle \bar{u}_i \rangle}{\partial x_j} + \frac{\partial \langle \bar{u}_j \rangle}{\partial x_i} \right) \frac{\langle \bar{u}_j \rangle}{Q} \right]. \tag{30}$$

With these closure assumptions, the final form of the modelled time-averaged, spatially-averaged NS equation [obtained by substituting Equations (22), (25) and (26) into Equations (19) and (20)] becomes

$$\frac{\partial\langle\bar{u}_j\rangle\langle\bar{u}_i\rangle}{\partial x_j} = -\frac{\partial\langle\bar{p}\rangle}{\partial x_i} + \frac{\partial}{\partial x_j}\left[(\nu+\nu_t)\left(\frac{\partial\langle\bar{u}_i\rangle}{\partial x_j}+\frac{\partial\langle\bar{u}_j\rangle}{\partial x_i}\right) - \frac{2}{3}\delta_{ij}\overline{\kappa}\right] - C_D\hat{A}\left[\left(Q+\frac{5}{3}\frac{\overline{\kappa}}{Q}\right)\langle\bar{u}_i\rangle - \nu_t\left(\frac{\partial\langle\bar{u}_i\rangle}{\partial x_j}+\frac{\partial\langle\bar{u}_j\rangle}{\partial x_i}\right)\frac{\langle\bar{u}_j\rangle}{Q}\right]. \tag{31}$$

Derivation of transport equations for $\overline{\kappa}$ and ϵ

The budget equations for $\overline{\kappa}$ and ϵ, which have been defined explicitly in Equations (23) and (24), need to be derived. To this purpose, let us define $f_i' \equiv f_i - \bar{f}_i$ as the fluctuating drag force. From Equations (28) and (29), we can derive

$$f_i' = -C_D\hat{A}Q\left(\frac{\langle\bar{u}_i\rangle\langle\bar{u}_k\rangle\langle u_k'\rangle}{Q^2} + \langle u_i'\rangle + \frac{\langle u_i'\rangle\langle\bar{u}_k\rangle\langle u_k'\rangle}{Q^2} - \frac{\langle\bar{u}_k\rangle}{Q^2}\overline{\langle u_i'\rangle\langle u_k'\rangle} + \frac{\langle\bar{u}_i\rangle\langle u_k'\rangle\langle u_k'\rangle}{2Q^2} - \frac{\langle\bar{u}_i\rangle\overline{\kappa}}{Q^2}\right). \tag{32}$$

The transport equation for the spatially-averaged fluctuating velocity $\langle u_i'\rangle$, obtained by subtracting the evolution equation for the time-averaged spatially-averaged velocity [Equation (19)] from the spatially-averaged Navier-Stokes equation [Equation (16)], can be written in symbolic form as follows:

$$\frac{D\langle u_i'\rangle}{Dt} = \cdots + f_i', \tag{33}$$

where D/Dt is the material derivative based on the spatially-averaged velocity $\langle u_i\rangle$. The time average of the linear combination $\langle u_j'\rangle D\langle u_i'\rangle/Dt + \langle u_i'\rangle D\langle u_j'\rangle/Dt$ gives the following transport equation for $\overline{\langle u_i'\rangle\langle u_j'\rangle}$:

$$\overline{\langle u_j'\rangle\frac{D\langle u_i'\rangle}{Dt} + \langle u_i'\rangle\frac{D\langle u_j'\rangle}{Dt}} = \frac{\bar{D}\overline{\langle u_i'\rangle\langle u_j'\rangle}}{\bar{D}t} = \cdots + F_{ij}, \tag{34}$$

where $\bar{D}/\bar{D}t$ is the material derivative based on the spatially-averaged, time-mean velocity $\langle\overline{u_i}\rangle$. Furthermore, F_{ij}, representing the interaction between the fluctuating drag force and spatially-averaged velocity fluctuations, has the explicit form

$$\begin{aligned} F_{ij} &\equiv \overline{\langle u_j'\rangle f_i' + \langle u_i'\rangle f_j'} \\ &= -C_D\hat{A}\left[2Q\overline{\langle u_i'\rangle\langle u_j'\rangle} + \frac{1}{Q}\left(\langle\bar{u}_i\rangle\langle\bar{u}_k\rangle\overline{\langle u_j'\rangle\langle u_k'\rangle} + \langle\bar{u}_j\rangle\langle\bar{u}_k\rangle\overline{\langle u_i'\rangle\langle u_k'\rangle}\right)\right. \\ &\quad + \frac{2}{Q}\langle\bar{u}_k\rangle\overline{\langle u_i'\rangle\langle u_j'\rangle\langle u_k'\rangle} \\ &\quad \left. + \frac{1}{2Q}\left(\langle\bar{u}_i\rangle\overline{\langle u_j'\rangle\langle u_k'\rangle\langle u_k'\rangle} + \langle\bar{u}_j\rangle\overline{\langle u_i'\rangle\langle u_k'\rangle\langle u_k'\rangle}\right)\right]. \end{aligned} \tag{35}$$

One-half the trace of F_{ij} yields

$$F \equiv \frac{1}{2}F_{ii} = \overline{\langle u_i' \rangle f_i'}$$
$$= -C_D \hat{A} \left[2Q\overline{\kappa} + \frac{1}{Q}\Big(\langle \bar{u}_i \rangle \langle \bar{u}_k \rangle \overline{\langle u_i' \rangle \langle u_k' \rangle} \Big) \right.$$
$$\left. + \frac{3}{2Q}\Big(\langle \bar{u}_k \rangle \overline{\langle u_i' \rangle \langle u_i' \rangle \langle u_k' \rangle} \Big) \right]. \tag{36}$$

The triple correlation term $\overline{\langle u_i' \rangle \langle u_i' \rangle \langle u_k' \rangle}$ in Equation (36) can be modelled, following Daly and Harlow [35], as

$$\overline{\langle u_i' \rangle \langle u_i' \rangle \langle u_k' \rangle} = 2C_s \frac{\overline{\kappa}}{\epsilon} \left[\overline{\langle u_k' \rangle \langle u_l' \rangle} \frac{\partial \overline{\kappa}}{\partial x_l} + \overline{\langle u_i' \rangle \langle u_l' \rangle} \frac{\partial \overline{\langle u_i' \rangle \langle u_k' \rangle}}{\partial x_l} \right], \tag{37}$$

where the closure constant $C_s \approx 0.3$ is used in the present study. This is a gradient transport model for the third moments of the spatially-averaged fluctuating velocity and involves a tensor eddy viscosity. In Equations (36) and (37), the double correlation $\overline{\langle u_i' \rangle \langle u_j' \rangle}$ was modelled previously using the constitutive relationship in Equation (22).

The transport equation for the time-averaged, sub-filter kinetic energy $\overline{\kappa}$ is obtained by multiplying Equation (33) by $\langle u_i' \rangle$ and time averaging the result. This procedure will give rise to the F term exhibited in Equation (36). This term represents the interaction of the flow with the obstacle elements and corresponds explicitly to the work done by the turbulence against the fluctuating drag force. The term F can be interpreted as an additional physical mechanism for the production/dissipation of $\overline{\kappa}$ associated with work against form and viscous drag on the obstacle elements. From this perspective, the exact transport equation for $\overline{\kappa}$ is

$$\langle \bar{u}_j \rangle \frac{\partial \overline{\kappa}}{\partial x_j} = -\frac{\partial T_j}{\partial x_j} - \overline{\langle u_i' \rangle \frac{\partial}{\partial x_j} \langle u_i'' u_j'' \rangle} + (P + F) - \epsilon, \tag{38}$$

where $F \equiv \overline{\langle u_i' \rangle f_i'}$; the flux T_j is

$$T_j \equiv \frac{1}{2}\overline{\langle u_j' \rangle \langle u_i' \rangle \langle u_i' \rangle} + \overline{\langle u_j' \rangle \langle p' \rangle} - \nu \frac{\partial \overline{\kappa}}{\partial x_j}; \tag{39}$$

and,

$$P \equiv -\overline{\langle u_i' \rangle \langle u_j' \rangle} \frac{\partial \langle \bar{u}_i \rangle}{\partial x_j} \tag{40}$$

is the production term (which is generally positive, and hence a 'source' in the $\overline{\kappa}$ equation). In addition to F, the exact transport equation for $\overline{\kappa}$ embodies an extra term represented by the second term on the right-hand-side of Equation (38). This term is the energy redistribution due to the interaction of the spatially-averaged velocity fluctuations with the gradient of the sub-filter stresses $\langle u_i'' u_j'' \rangle$.

The modelled transport equation for $\overline{\kappa}$ is then obtained as follows. Firstly, the additional energy redistribution term identified above is assumed to be negligible, and will be ignored henceforth. Secondly, the energy flux T_j is modelled with a gradient diffusion hypothesis

$$T_j = -\frac{\nu_t}{\sigma_k} \frac{\partial \overline{\kappa}}{\partial x_j}, \tag{41}$$

where the 'turbulent Prandtl number' for $\overline{\kappa}$ is assumed to be $\sigma_k = 1$. Thirdly, the additional physical effect on $\overline{\kappa}$ due to viscous and form drag on the obstacle elements embodied in $F \equiv \overline{\langle u_i' \rangle f_i'}$ will be modelled using Equations (36) and (37). With these closure approximations, the model transport equation for $\overline{\kappa}$ assumes the form

$$\frac{\partial \langle \bar{u}_j \rangle \overline{\kappa}}{\partial x_j} = \frac{\partial}{\partial x_j}\left(\frac{\nu_t}{\sigma_k}\frac{\partial \overline{\kappa}}{\partial x_j}\right) + (P + F) - \epsilon, \tag{42}$$

where the explicit form for F is exhibited in Equations (36) and (37).

The exact transport equation for ϵ can be derived rigorously, but it is not a useful starting point for a model equation. Consequently, rather than being based on the exact equation, the model equation for ϵ here is essentially a dimensionally consistent analog to the $\overline{\kappa}$-equation. In this sense, the model equation for ϵ is best viewed as being entirely empirical. To this purpose, we note that the time scale $\tau \equiv \overline{\kappa}/\epsilon$ will make the production and dissipation terms in the $\overline{\kappa}$-equation dimensionally consistent. Hence, the dimensionally consistent analog to Equation (42) becomes

$$\frac{\partial \langle \bar{u}_j \rangle \epsilon}{\partial x_j} = \frac{\partial}{\partial x_j}\left(\frac{\nu_t}{\sigma_\epsilon}\frac{\partial \epsilon}{\partial x_j}\right) + \frac{\epsilon}{\overline{\kappa}}\left(C_{\epsilon 1}(P + F) - C_{\epsilon 2}\epsilon\right), \tag{43}$$

where $\sigma_\epsilon = 1.3$, $C_{\epsilon 1} = 1.44$ and $C_{\epsilon 2} = 1.92$ are empirical (closure) constants. The ϵ-equation here essentially retains the same form as the usual model equation for ϵ commonly utilized in the standard k-ϵ model [34]. The only difference here is that the drag force effect on the turbulence (embodied in the term F) has been included with the production term P in Equation (43).

In Equation (43), we have grouped F with P in the ϵ-equation. In other words, we sensitize the ϵ-equation to the effects of form and viscous drag of the obstacle elements by replacing P with $P + F$ in the 'production of dissipation' term (usually, the effect of the obstacle elements is to enhance the dissipation in the canopy airspace). This treatment is similar to the rationale used by Ince and Launder [36] for dealing with buoyancy effects on turbulence in buoyancy-driven flows. In these types of flows, the gravitational production term $G \equiv -\beta g_i \overline{u_i' T'}$ (g_i is the gravitational acceleration vector, β is the thermal expansion coefficient, and T' is the virtual temperature fluctuation) is included with P in the transport equation for the viscous dissipation rate. In this regard, our proposed approach for treating F in the ϵ-equation differs from that suggested by Getachew et al. [33].

Wake production

The closure of the spatially-averaged RANS equation [cf. Equations (11) and (12)] requires a transport equation for $\langle k \rangle \equiv \frac{1}{2}\langle \overline{u_i' u_i'} \rangle$ (i.e., the spatially-averaged turbulence kinetic energy), whereas that for the time-averaged spatially-averaged NS equation [cf. Equations (19) and (20)] requires a transport equation for $\overline{\kappa} \equiv \frac{1}{2}\overline{\langle u_i' \rangle \langle u_i' \rangle}$ (i.e., the time-averaged sub-filter kinetic energy). The model transport equation for $\overline{\kappa}$ in Equation (42) included a source/sink term F whose form can be systematically derived in terms of the drag force term that appears in the mean momentum equation [cf. Equation (36)].

The budget equation for $\langle k \rangle$ can be derived by applying the spatial averaging operator to the standard transport equation for k to give

$$\langle \bar{u}_j \rangle \frac{\partial \langle k \rangle}{\partial x_j} = -\langle \overline{u_i' u_j'} \rangle \frac{\partial \bar{u}_i}{\partial x_j} - \frac{\partial}{\partial x_j} \left[\frac{1}{2} \langle \overline{u_j' u_i' u_i'} \rangle + \langle \overline{u_j' p'} \rangle + \underbrace{\frac{1}{2} \langle \bar{u}_j'' \overline{u_i' u_i'} \rangle}_{\text{I}} \right] + \nu \frac{\partial^2 \langle k \rangle}{\partial x_j^2} - \varepsilon - \underbrace{\left\langle \overline{u_i' u_j'}'' \frac{\partial \bar{u}_i''}{\partial x_j} \right\rangle}_{\text{II}}. \tag{44}$$

In Equation (44), $\varepsilon \equiv \nu \langle \overline{\frac{\partial u_i'}{\partial x_j} \frac{\partial u_i'}{\partial x_j}} \rangle$ is the isotropic turbulent dissipation rate for $\langle k \rangle$.

The transport equation for $\langle k \rangle$ contains two additional terms (designated I and II) that need to be approximated. Term I corresponds to the dispersive transport of $\langle k \rangle$ [analogous to the dispersive flux of momentum in Equations (11) and (12)]. Term II can be identified as a wake production term (see Raupach and Shaw [14]) which accounts for the conversion of mean kinetic energy to turbulent energy in the obstacle wakes by working of the mean flow against the drag. This term is analogous to the F term that appears in the transport equation for $\overline{\kappa}$, but unlike F whose form can be systematically derived from the form and viscous drag force term that appears in the mean momentum equation, the link (if any) between the wake production term in Equation (44) and the drag force term in the mean momentum equation is less obvious. For example, Raupach and Shaw [14] showed that provided (1) the dispersive stress $\langle \bar{u}_i'' \bar{u}_j'' \rangle$ and the dispersive transport of $\langle k \rangle$ are both negligible and (2) the mean kinetic energy is not directly dissipated to heat in the canopy, the wake production term can be approximated as follows:

$$-\left\langle \overline{\left(\overline{u_i' u_j'}\right)}'' \frac{\partial \bar{u}_i''}{\partial x_j} \right\rangle = -\langle \bar{u}_i \rangle \bar{f}_i = 2 C_D \hat{A} Q \underbrace{\left(\frac{1}{2} \langle \bar{u}_i \rangle \langle \bar{u}_i \rangle \right)}_{K}, \tag{45}$$

where K represents the mean kinetic energy (kinetic energy of the spatially-averaged time-mean flow). Note that use of Equation (45) as a model for the wake production term strictly provides a source term in the transport equation for $\langle k \rangle$.

However, Green [21] and Liu et al. [24] found that it was important to include also a sink term in the budget equation for $\langle k \rangle$ and. to this purpose, modelled the wake production term in the budget equation for $\langle k \rangle$ in an *ad hoc* manner as

$$-\left\langle \overline{\left(\overline{u_i' u_j'}\right)}'' \frac{\partial \bar{u}_i''}{\partial x_j} \right\rangle = 2 C_D \hat{A} Q \underbrace{\left(\frac{1}{2} \langle \bar{u}_i \rangle \langle \bar{u}_i \rangle \right)}_{K} - 4 C_D \hat{A} Q \underbrace{\left(\frac{1}{2} \langle \overline{u_i' u_i'} \rangle \right)}_{\langle k \rangle}, \tag{46}$$

which includes a gain to $\langle k \rangle$ from conversion of the mean kinetic energy K to turbulence energy at the larger scales (source term) and a loss from $\langle k \rangle$ of the large-scale turbulence energy to smaller (wake) scales (sink term). More specifically, Green [21] argued heuristically that the sink term in Equation (46) was required to account for the accelerated cascade of $\langle k \rangle$ from large to small scales due to the presence of the roughness elements (arising from

the rapid dissipation of fine-scale wake eddies in a plant canopy). Liu et al. [24] noted that the *ad hoc* inclusion of the sink term (second term on the right-hand side) of Equation (46) [which was inserted in hindsight] was important, for otherwise they found that their predicted $\langle k \rangle$ was "about 100% larger than the experimental measurements when the second term was ignored".

In contrast, the additional source/sink term F that appears in the budget equation for $\overline{\kappa}$ can be systematically derived from rate of working of the turbulent velocity fluctuations against the fluctuating drag force, and appears naturally in the derivation of the budget equation for $\overline{\kappa}$. Even though the 'turbulence kinetic energy' $\overline{\kappa} \equiv \frac{1}{2}\overline{\langle u_i' \rangle \langle u_i' \rangle}$ (time-averaged, sub-filter kinetic energy) used in our turbulence closure model is different from the usual form of the spatially-averaged turbulence kinetic energy $\langle k \rangle \equiv \frac{1}{2}\langle \overline{u_i' u_i'} \rangle$, they are nevertheless related as follows:

$$\langle k \rangle - \overline{\kappa} = \frac{1}{2}\Big(\langle \overline{u_i'' u_i''} \rangle - \langle \bar{u}_i'' \bar{u}_i'' \rangle \Big) = \frac{1}{2}\langle \overline{(u_i')'' (u_i')''} \rangle. \tag{47}$$

Note that the difference between $\langle k \rangle$ and $\overline{\kappa}$ is proportional to the difference between the two forms of dispersive stress that appear in the spatially-averaged RANS equation and the time-averaged, spatially-averaged NS equation. However, note that this difference can be expressed as the spatial average of time averages of the departures of velocity fluctuations from their spatial (volume) average. Since this term involves a "perturbation of a perturbation", it seems reasonable to *assume* that

$$0 \approx \frac{1}{2}\Big| \langle \overline{(u_i')'' (u_i')''} \rangle \Big| \ll \max\big(\langle k \rangle, \overline{\kappa} \big). \tag{48}$$

With this assumption, $\langle k \rangle$ and $\overline{\kappa}$ are expected to be almost equal in value (viz., $\langle k \rangle \approx \overline{\kappa}$). This, together with Equation (21), also implies that

$$\langle \bar{u}_i'' \bar{u}_j'' \rangle \approx \langle \overline{u_i'' u_j''} \rangle, \tag{49}$$

or, in other words, the dispersive stresses are expected to be approximately equal to the spatial average of the high-frequency turbulent stresses. Finally, with reference to Equation (21), this implies that $\overline{\langle u_i' \rangle \langle u_j' \rangle} \approx \langle \overline{u_i' u_j'} \rangle$. The latter approximation will be used in a later section to compare model predictions of $\overline{\langle u_i' \rangle \langle u_j' \rangle}$ with the diagnosed values of $\langle \overline{u_i' u_j'} \rangle$ obtained from a high-resolution RANS simulation.

Interestingly, the 'zeroth-order' term in our expansion of F in Equation (36) rewritten below

$$F \equiv \overline{\langle u_i' \rangle f_i'} = -2 C_D \hat{A} Q \underbrace{\left(\frac{1}{2}\overline{\langle u_i' \rangle \langle u_i' \rangle} \right)}_{\overline{\kappa}} + \text{H.O.T},$$

where H.O.T denotes higher-order correction terms, is analogous to the sink term contribution for the wake production term in Equation (46) [except the factor here is 2, rather than 4]. Note that the higher-order correction terms for F can have either sign implying that they are source/sink terms. More importantly, it needs to be emphasized that the leading-order term of F is a *sink* term, and not a source term implying that in the transport equation for $\overline{\kappa}$ the conversion of MKE to TKE is *ipso facto* absent.

Determination of drag coefficient

In this section, we will explicitly diagnose a drag coefficient C_D using the results for a high-resolution CFD simulation of a developing flow over an aligned array of cubes (3-D buildings) (described in I). This regular building array consisted of seven rows of cubes arranged with a plan area density of 0.25 [28]. To derive a drag coefficient for this array, first note from Equations (13) and (29) that the x-component of the drag force $\bar{f}_i$ ($i = 1 \equiv x$) reduces to

$$\bar{f}_x \equiv \frac{\nu}{V}\int_S \frac{\partial \bar{u}}{\partial n} dS - \frac{1}{V}\int_S \bar{p} n_x dS = -C_D(z)\hat{A}Q\langle\bar{u}\rangle, \tag{51}$$

where we assume implicitly that V in Equation (51) is a thin horizontal slab centered at the level z.

To specialize the analysis to the aligned 3-D building array consisting of the 7 rows of cubes arranged normal to the mean wind direction, we consider decomposing this array into seven "drag units" as illustrated in Figure 1(a). Each drag unit consists of one row of cubes (buildings) and the associated downstream street canyon. To diagnose a drag coefficient $C_D(z)$ at level z for each drag unit in the array, we take an averaging volume V as the thin horizontal slab shown in Figure 1(b). Now application of Equation (51) to this averaging volume gives the following explicit expression for the pressure drag:

$$-\frac{1}{V}\int_S \bar{p} n_x dS = -\frac{1}{2H^2}\left[\int_0^{H/2} \left(\bar{p}|_{x=x0} - \bar{p}|_{x=x0+H}\right) dy\right]. \tag{52}$$

The frictional drag, $\frac{\nu}{V}\int_S \frac{\partial \bar{u}}{\partial n} dS$, can be evaluated similarly using the 'wall function' approach to estimate the skin friction along the building surfaces [37]. With the computation of the pressure and frictional drag forces, the local or sectional drag coefficient $C_D(z)$ can then be diagnosed as follows [cf. Equation (51)]:

$$C_D(z)\hat{A} = \frac{-\bar{f}_x}{\max\left(\delta, Q\langle\bar{u}\rangle(z)\right)}, \tag{53}$$

where $\delta \approx 0.0025 \ll 1$ is chosen here to avoid a possible singularity problem for the case when $\langle\bar{u}\rangle \approx 0$. We note that the results to be shown in the next section are insensitive to the exact value chosen for δ in Equation (53). Furthermore, for developing flow over a building array, a local equilibrium assumption involving the balance between the obstacle drag force and the downward transport of momentum by turbulent stresses cannot be used to diagnose the sectional drag coefficient.

Vertical profiles of $C_D(z)$ over the range of heights $0 \leq z/H \leq 1$ for each drag unit in the 3-D building array are shown in Figure 2. For the first drag unit (associated with the first row of buildings in the array), $C_D(z)$ increases monotonically with decreasing z/H. For drag units in the array interior (drag unit #3 or greater), $C_D(z)$ first increases, then decreases. and then increases again with decreasing z/H. In all cases, the highest values of $C_D(z)$ were obtained near the ground as $z/H \to 0$, with $C_D(z)$ decreasing to a small value at the top of the canopy, the latter of which implies a significant reduction in the rearward pressure deficit near the canopy top.

We note that C_D is smaller for the drag units in the interior of the building array compared to that of the first drag unit which is influenced by the impingement region upwind of the array. This is an example of the 'shelter effect' where the mutual interference of the obstacle elements leads to a reduction in the value of the drag coefficient measured *in situ* within the array compared to the drag coefficient measured in the free-stream flow (e.g., drag coefficient corresponding to drag unit #1). Indeed, the largest value of the sectional drag coefficient $C_D(z)$ at a given z occurs in drag unit #1 (i.e.. first row of buildings) over much of the canopy depth. This first drag unit is responsible primarily for the adverse pressure gradient in the impingement zone upwind of the building array that results in a significant deceleration of the air flow here. In contrast, the smallest value of the drag coefficient $C_D(z)$ at each level z/H occurs for drag unit #2 which corresponds to the region in the building array (viz., in the immediate leeward zone of the first row of buildings) where the shelter effect is most pronounced. More specifically, the maximum mean wind speed and turbulence reduction occurs in this immediate leeward 'quiet' zone (corresponding to drag unit #2).

Because such detailed information on the sectional (local) drag coefficient is not usually available, it is useful to consider also the application of a bulk drag coefficient. To this purpose, we consider three different methods for the evaluation of a bulk drag coefficient, $C_{D,\text{bulk}}$. These three methods for determination of a bulk drag coefficient are defined as follows:

Method 1:

$$C_{D,\text{bulk},i} = \frac{1}{H}\int_{z=0}^{z=H} C_D(z)dz, \tag{54}$$

where $C_{D,\text{bulk},i}$ $(1 \leq i \leq 7)$ is the bulk drag coefficient for each drag unit determined by averaging the sectional drag coefficient at height z $(C_D(z))$ over the entire depth of the canopy;

Method 2:

$$C_{D,\text{bulk,ave}} = \frac{1}{7}\sum_{i=1}^{7} C_{D,\text{bulk}.i}, \tag{55}$$

is the arithmetic average of $C_{D,\text{bulk},i}$ over the drag units comprising the entire 3-D building array; and,

Method 3:

$$C_{D,\text{bulk},1} \equiv C_{D,\text{bulk},i}|_{i=1} \tag{56}$$

is the bulk drag coefficient for the first drag unit. This is similar to using a drag coefficient diagnosed for the flow over a single (isolated) row of buildings (viz., a free-stream bulk drag coefficient).

The variation of the bulk drag coefficient $C_{D,\text{bulk}.i}$ (defined using Method 1 above) with increasing drag unit i in the array (viz., with increasing fetch through the urban canopy) is exhibited in Figure 3(a). Here, we have decomposed the drag coefficient $C_{D,\text{bulk},i}$ into a contribution from the form (pressure) drag $C_{Dp,\text{bulk}.i}$ and the frictional (viscous) drag $C_{Df,\text{bulk},i}$. Note that the contribution of the frictional (viscous) drag $(C_{Df,\text{bulk}})$ to the bulk drag coefficient is negligible in comparison with the contribution from the pressure (form) drag $C_{Dp,\text{bulk}}$. Generally, the contribution of the skin friction to the bulk drag coefficient is less than one percent of the contribution of the form drag. We note that the

bulk drag coefficient for drag units in the array interior (viz., for drag unit #3 or greater) is between one-half and two-thirds of the bulk drag coefficient for drag unit #1 (viz., drag unit associated with the row of buildings forming the upstream boundary of the array) implying a 'shelter factor' (ratio of free-stream bulk drag coefficient to the *in situ* value) of between about 1.5 and 2. This is consistent with the reported range of shelter factors of between 1 to 4 compiled by Raupach and Thom [38] in their review of canopy flows. Finally, the bulk drag parameters $C_{D,\text{bulk,ave}}\hat{A}$ and $C_{D,\text{bulk,1}}\hat{A}$ were found to be about 0.7 and 1.2, respectively [cf. Figure 3(b)] for the 3-D building array considered here.

Results and discussion

The results to be presented in this section were obtained with three different versions of the k-ϵ model (distinguished by the source/sink terms included in the transport equations for k and ϵ) with the major differences between these versions summarized below.[2]

Model (Version) 1: Model 1 is in essence the same as the proposed model except that $\bar{f}_i$ in Equation (30) is replaced by

$$\bar{f}_i = -C_D\hat{A}Q\langle\bar{u}_i\rangle, \tag{57}$$

and F in Equation (36) is set identically to zero. Hence, in this version of the model, no additional source or sink terms are included in the transport equations for k and ϵ, and a simplified parameterization for the mean drag force vector [viz. Equation (57)] is used.

Model (Version) 2: Model 2 is Lee and Howell's model [39], in which the parameterization for the mean drag force vector $\bar{f}_i$ is that displayed in Equation (57). However, unlike Model 1, the leading order term of F in Equation (36) is retained (viz., a sink term of the form $F \approx -2C_D\hat{A}Q\bar{\kappa}$ is incorporated into the transport equation for $\bar{\kappa}$). Finally, rather than include this leading order approximation of F with the production term P as in Equation (42), Lee and Howell's model introduces a sink term of the form $\epsilon F/\bar{\kappa} \approx -2C_D\hat{A}Q\epsilon$ into the transport equation for ϵ. However, we note that the inclusion of the 'zeroth-order' approximation for F here with the production term P in the ϵ-transport equation [cf. Equation (42)] did not make a significant difference in the flow predictions (viz., the predictions of urban flow using the latter model are indistinguishable from those obtained using Lee and Howell's model).

Model (Version) 3: Model 3 is the current model (described above), consisting of Equations (31), (36), (37), (40), (42), and (43).

The $\bar{\kappa}$-isopleths predicted by three different models (summarized above) using the local (sectional) drag coefficient $C_D(z)$ (cf. Figure 2) are displayed in Figure 4. As the upstream flow impinges on the leading edge of the building array, which is modelled here as a 'porous layer' of height H extending from the upstream edge of the first drag unit to the downstream edge of the last drag unit, the deceleration of the flow within the volume of the canopy ($z/H < 1$) and acceleration (overspeeding) of the flow above about $z/H \approx 4/3$ results in a

[2] Although we use the standard terminology in k-ϵ closure modelling and refer to the transport equation for the turbulence energy as the k-equation, this should be interpreted more precisely here to refer actually to the transport equation for $\overline{\kappa}$ (viz., the time-averaged, sub-filter kinetic energy). Consequently, in this section, the k-equation will be interpreted to be synonymous with the $\overline{\kappa}$-equation, so that k and $\overline{\kappa}$ will be used interchangeably in what follows.

strong shear in the mean flow in the region of the canopy top. An inflection point occurs in the mean wind at $z/H \approx 1$ where the mean shear $\partial\langle\bar{u}\rangle/\partial z$ assumes its maximum value. This mean shear acts as a source for the generation of k through $P \sim \left(\partial\langle\bar{u}\rangle/\partial z\right)^2$ (in the Boussinesq eddy-viscosity approximation) at or near the top of the canopy. The presence of an inflection point in the mean velocity profile and the strong generation of k in the region of the inflection point is characteristic of a plane mixing layer (i.e., a free shear layer that forms when two airstreams of different velocities, initially separated, merge downstream of the separation and interact) as discussed by Raupach et al. [40] for the case of plant canopies.

A perusal of the results in Figure 4 shows that Model 1 performs significantly differently than the other two models. In particular, Model 1 exhibits a much more prominent turbulence kinetic energy (TKE) 'plume' than is evident in the other 2 models. This TKE 'plume' originates from the upstream rooftop edge of the first building and spreads vertically at a constant (approximately or better) rate, achieving a vertical depth of about $5H$ at roughly a downstream distance of $25H$ from the upstream edge of the building array. The TKE 'plume' is advected by the fluid flow in the downstream direction, and its rate of spread in the vertical direction is governed by turbulence diffusion through the eddy viscosity $\nu_t \sim k^2$. For Model 1, no drag-force-related 'sink' terms are included in the k- and ϵ-equations, resulting in an excessive level of k and, hence, ν_t. This, in turn, increases the spreading rate of the TKE 'plume'. In contrast, the turbulence energy levels predicted by Models 2 and 3 (which incorporate minimally an additional sink term in the k- and ϵ-equations) are smaller than those predicted by Model 1. Furthermore, Model 1 also predicts a much higher level of k within the volume of the canopy (particularly in the near wall region $0 \leq z/H \lesssim 0.5$) than Models 2 or 3. In general, the prediction of turbulence energy provided by Models 2 and 3 is similar except for the region downstream of the leeward rooftop edge of the last building ($14 \lesssim x/H \lesssim 17.5$) where Model 3 predicts a slightly higher level of k than Model 2. It appears from this observation that k is not very sensitive to the differing treatments of sources and sinks in the k- and ϵ-equations, while simulations using the k-ϵ closure without additional sources and sinks in the k- and ϵ-equations lead to significantly different predictions of the turbulence energy levels.

Profiles of predicted spatially-averaged time-mean streamwise velocity $\langle\bar{u}\rangle$ obtained using Models 1–3 for the first six drag units are shown in Figure 5. These predictions are compared to $\langle\bar{u}\rangle$ obtained by spatially-averaging RANS mean flow solutions over the same volumes occupied by the drag units. Our high-resolution RANS simulations of the 3-D building array considered here are reported in I. The latter results, which have been spatially-averaged here, will be labelled in the figures using the symbol 'o' and will be referred to henceforth as 'high-resolution CFD' results. Within the volume of the canopy, the spatially-averaged time-mean velocity predicted by Models 2 and 3 (cf. Figure 5) are in excellent agreement with the high-resolution CFD results for drag units #3 to #6. However, for the first two drag units, $\langle\bar{u}\rangle$ is slightly overpredicted by these two models which appears to be a result of the severe underestimation of $\overline{\langle u'\rangle\langle u'\rangle}$ in the near-wall region $z/H \lesssim 2/3$ (see below). Vertical profiles of $\langle\bar{u}\rangle$ obtained from the high-resolution CFD results appear to have reached streamwise equilibrium (viz.. the spatially-averaged, time-mean streamwise velocity field is fully developed) by the third drag unit, a feature that is reproduced correctly by all three models.

The corresponding profiles of turbulence quantities $\overline{\langle u' \rangle \langle u' \rangle}$ (streamwise normal stress) and $\overline{\langle u' \rangle \langle w' \rangle}$ (shear stress) are displayed in Figures 6 and 7, respectively. Consistent with Figure 4 in relation to the spreading of the TKE 'plume', the peak values of $\overline{\langle u' \rangle \langle u' \rangle}$ (i.e., the streamwise normal stress component of k) at $z/H \approx 4/3$ are overpredicted by all three models. This overprediction of $\overline{\langle u' \rangle \langle u' \rangle}$ is rather significant for Model 1, particularly in drag units #2 to #6. An overestimation of $\overline{\langle u' \rangle \langle u' \rangle}$ (and, by inference of k) gives too high values of the eddy viscosity $\nu_t \sim k^2$, yielding an excessive vertical turbulent diffusion of mean momentum. This, in turn, results in an underestimation of the magnitude of the mean shear at the top of the canopy and an underprediction of $\langle \bar{u} \rangle$ in the region above the canopy height (i.e., in $z/H \gtrsim 1$).

The vertical spreading of the TKE 'plume' is evident on an examination of the streamwise development of $\overline{\langle u' \rangle \langle u' \rangle}$ in Figure 6. Here, it is seen that $\overline{\langle u' \rangle \langle u' \rangle}$ approaches its undisturbed far upstream value at the level of $z \approx 350$ mm ($z/H \approx 2.3$) in drag unit #1, but at the greater level of $z \approx 500$ mm ($z/H \approx 3.3$) in drag unit #6. Interestingly, the peak value of $\overline{\langle u' \rangle \langle u' \rangle}$ also *increases* monotonically in the streamwise direction, which is markedly different from what we normally would expect from the development of a mixing layer (assuming that the shear flow near the canopy top has the characteristics of a plane mixing layer). For example, in Model 1, the peak value of $\overline{\langle u' \rangle \langle u' \rangle}$ is ≈ 0.3 m^2 s^{-2} in drag unit #1 and ≈ 0.5 m^2 s^{-2} in drag unit #6. However, the high-resolution CFD results show almost no tendency of streamwise development in the streamwise normal stress after drag unit #3, which is consistent with the streamwise variation of $C_{D,\text{bulk}}$ displayed previously in Figure 3. In particular, within the array interior ($x/H \gtrsim 6$), it appears that the flow statistics (mean flow and turbulence) within the third street canyon should be "typical" of their neighbors, implying that in the array interior a periodic boundary condition could have been imposed to model the flow within a unit drag cell consisting of a single row of 3-D buildings and the associated street canyon.

The deficiency of not being able to predict a fully-developed state for the turbulence fields within the array using a distributed drag force approach might be due to the defects in the F term included in the transport equation for k. Although in the present model, higher-order corrections to the nonlinear drag force term, similar to those proposed by Getachew et al. [33] have been included, their overall effect on the model prediction does not appear to be significant. Indeed, the model predictions obtained with the more complex model proposed here is not significantly different from the simpler Lee and Howell model [39]. However, the effectiveness of the higher-order corrections in our model, particularly the triple correlations $\overline{\langle u_i' \rangle \langle u_i' \rangle \langle u_k' \rangle}$, can only probably be realized if the Reynolds stress anisotropy can be correctly represented, which is difficult to achieve within the present impoverished k-ϵ modelling framework used in conjunction with the Boussinesq linear stress-strain relationship.

As the major component in P is $-\overline{\langle u' \rangle \langle w' \rangle} \partial \langle \bar{u} \rangle / \partial z$, we expect the shear stress $-\overline{\langle u' \rangle \langle w' \rangle}$ to be overestimated by the three models in order to be consistent with the overestimation of k and $\overline{\langle u' \rangle \langle u' \rangle}$ observed in Figures 4 and 6. It is seen in Figure 7 that Model 1 predicts a peak value in shear stress that is approximately 4–5 times smaller (i.e., more negative) than the high-resolution CFD results for drag units #1 to #6. Even for Models 2 and 3, the peak values of $\overline{\langle u' \rangle \langle w' \rangle}$ are still too small (i.e., too negative), although Model 2 performs slightly better than Model 3 in the prediction of $\overline{\langle u' \rangle \langle w' \rangle}$ and $\overline{\langle u' \rangle \langle u' \rangle}$ (cf. Figure 6). However, it should be emphasized here that the true performance of the present model can only be

assessed if a higher-order closure model, such as the Reynolds stress transport model of Launder et al. [41] that is capable of predicting the anisotropy of the turbulence fields, is used. This is an interesting topic for a future investigation.

The effect of the specification of C_D on the predictive performance of a distributed drag force model will be investigated. To this purpose, the diagnosed sectional drag coefficient (cf. Figure 2) and three bulk drag coefficients (cf. Figure 3) have been used as input to Model 3 for the prediction of $\langle\bar{u}\rangle$, $\overline{\langle u'\rangle\langle u'\rangle}$, and $\overline{\langle u'\rangle\langle w'\rangle}$. The results of this simulation are displayed in Figures 8, 9, and 10. It is seen from Figure 8 that the use of a sectional drag coefficient $C_D(z)$ permitted a more accurate prediction of $\langle\bar{u}\rangle$ in drag unit #1 for the region $z/H \lesssim 2/3$. This is the result of the correct representation in the increase of the drag coefficient with decreasing z/H which is embodied in the local drag coefficient, but is missing in the representation provided by the bulk drag coefficients. Nevertheless, the predictive performance of the model using only the bulk drag coefficients generally gave similar results to those obtained with the sectional drag coefficient for both the mean flow and turbulence.

For drag unit #2, it is observed that the model prediction for $\langle\bar{u}\rangle$ below the canopy height obtained using the bulk drag coefficient $C_{D,\text{bulk},1}$ is markedly different from the other three sets of predictions obtained using $C_D(z)$, $C_{D,\text{bulk},i}$, and $C_{D,\text{bulk,ave}}$. More specifically, $\langle\bar{u}\rangle$ is too small (i.e., underpredicted) for $2/5 \lesssim z/H \lesssim 1$ compared to the high-resolution CFD results. This is because $C_{D,\text{bulk},1}$ can be regarded as the drag coefficient for a flow over an *isolated* row of cubical buildings (i.e., a free-stream drag coefficient). The drag of an isolated row of buildings is different from its effective drag *in situ* (viz., the drag of a row of buildings within a building array, where the 'shelter effect' becomes important). It was shown earlier that the drag for a row of buildings (modelled as a porous barrier here) *in situ* is less than for the same row of buildings in isolation owing to the 'shelter effect'. In fact, the current calculations show that the drag coefficient drops considerably after the first row of buildings in the array due to the 'shelter effect' and recovers rapidly thereafter, reaching approximately its fully-developed value somewhere between the third and fourth rows of buildings in the array (cf. Figure 3).

Overall, good predictions of the mean flow through the canopy, except in drag unit #1, can be achieved by the using $C_{D,\text{bulk,ave}}$, the latter of which can be considered to be equal (approximately or better) to the fully-developed value of $C_{D,\text{bulk}}$ in the array interior. Since $C_D(z)$ and $C_{D,\text{bulk},i}$ are difficult to obtained in practice, we recommend the approach of using $C_{D,\text{bulk},1}$ (free-stream drag coefficient) for drag unit #1 and $C_{D,\text{bulk,ave}}$ for all other drag units in the array (all of which will 'experience' some form of sheltering from the drag unit(s) upstream of it). Both $C_{D,\text{bulk},1}$ and $C_{D,\text{bulk,ave}}$ are simpler to obtain experimentally than the sectional drag coefficient $C_D(z)$.

Conclusions

The present k-ϵ model was derived rigorously based on a time-averaging of the spatially-averaged NS equation. If we assume that the kinematic dispersive stresses, $\langle\bar{u}_i''\bar{u}_j''\rangle$, are comparable in magnitude to $\overline{\langle u_i''u_j''\rangle}$ [an explicit demonstration of the validity of this assumption will require either a Direct Numerical Simulation (DNS) or a Large Eddy Simulation (LES)], then $\overline{\langle u_i'\rangle\langle u_j'\rangle}$ can be compared directly with the spatially-averaged kinematic

Reynolds stresses, $\langle\overline{u_i'u_j'}\rangle$, the latter of which can be estimated explicitly using the high-resolution CFD results presented in I (or, equivalently, $\overline{\kappa}$ can be compared directly to $\langle k\rangle$, the latter quantity of which is available directly from a RANS simulation).

We found that the peak of the kinematic streamwise normal stress, $\overline{\langle u'\rangle\langle u'\rangle}$, was overpredicted by all three models investigated here. However, we note that these models overpredict $\overline{\langle u'\rangle\langle u'\rangle}$ (and, by inference, $\overline{\kappa}$) when compared to the high-resolution CFD results, the latter of which are assumed implicitly to correspond to the "ground truth". However, this may not necessarily be the "correct" comparison since it was shown in I that the RANS simulation generally gave an underprediction of the turbulence energy in the building array, implying that the spatially-averaged TKE obtained from these high-resolution CFD simulations will probably underpredict the true (but unknown) values. Hence, the overprediction of the streamwise normal stress by the distributed drag force models may not be as severe as apparently indicated here in comparison with the high-resolution CFD results.

Nevertheless, Model 1 (i.e., model with no additional source/sink terms in the k- and ϵ-equations) gave the worst predictive performance of the three models considered. Model 2 (Lee and Howell's model) and Model 3 (current proposed model) gave very similar predictions for the mean streamwise velocity $\langle\bar{u}\rangle$. In terms of turbulence quantities (viz., $\overline{\langle u'\rangle\langle u'\rangle}$ and $\overline{\langle u'\rangle\langle w'\rangle}$), Model 2 gave slightly better results than Model 3, which appears to suggest that the contribution of the higher-order correction terms in the present model, displayed in the F term of Equation (36), is not important. In other words, the predictions of the turbulence quantities do not appear to be sensitive to the precise treatment of the source and sink terms in the k- and ϵ-equations. However, it is possible that the insensitivity of the results to the inclusion of such higher-order terms in the model is caused by the use of the Boussinesq linear stress-strain constitutive relation [i.e., Equation (22)] within the k-ϵ modelling framework. Hence, higher-order turbulence closure models, such as the Reynolds stress transport model of Launder et al. [41] that is capable of predicting the anisotropy in the Reynolds stress field, might be required here in order to take full advantage of the higher-order correction terms.

The profiles of $\langle\bar{u}\rangle$ are in general well predicted by the present model in conjunction with the use of a sectional drag coefficient $C_D(z)$, or the bulk drag coefficients $C_{D,\text{bulk},i}$ and $C_{D,\text{bulk,ave}}$, particularly, below the canopy height ($z/H \leq 1$). However, when $C_{D,\text{bulk},1}$ was used, the $\langle\bar{u}\rangle$-profiles within the canopy were generally underpredicted (at least for the first four drag units of the array) due to the neglect of the 'shelter effect' in the canopy interior. In consequence, we recommend that in modelling of the developing flow over a building array using the distributed drag force approach that $C_{D,\text{bulk},1}$ (or, equivalently, the free-stream drag coefficient) be assigned to the first drag unit (e.g., first row of buildings in the array) and $C_{D,\text{bulk,ave}}$ (or, equivalently, an *in situ* drag coefficient for the fully-developed flow in the array interior) be assigned to the remaining drag units.

References

1. Smith, W. S., Reisner, J. M., DeCroix, D. S., Brown, M. J., Lee, R. L., Chan, S. T. and Stevens, D. E. (2000). A CFD Model Intercomparison and Validation Using High Resolution Wind Tunnel Data. *11th Joint Conference on the Applications of Air Pollution Meteorology with the A&WMA*, American Meteorological Society, Boston, MA, 41–46.

2. DeCroix, D. S., Smith, W. S., Streit, G. E. and Brown, M. J. (2000). Large-Eddy and Gaussian Simulations of Downwind Dispersion From Large Building HVAC Exhaust. *11th Joint Conference on the Applications of Air Pollution Meteorology with the A&WMA*, American Meteorological Society, Boston, MA, 53–58.

3 Lien, F. S., Yee, E. and Cheng, Y. (2003). Simulation of Mean Flow and Turbulence Over a 2-D Building Array Using High-Resolution CFD and a Distributed Drag Force Approach. *J. Wind Eng. Ind. Aerodyn.*, 92, 117–158.

4 Yee, E. and Lien, F. S. (2004). Numerical Simulation of the Disturbed Flow Through a Three-Dimensional Building Array. DRDC Suffield TR 2004–108, Defence R&D Canada – Suffield, 68 pp.

5. Wilson, J. D. and Yee, E. (2000). Wind Transport in an Idealized Urban Canopy. *3rd Symposium on the Urban Environment*, American Meteorological Society, Davis, CA, 40–41.

6. Raupach, M. R., Coppin, P. A. and Legg, B. J. (1986). Experiments on Scalar Dispersion Within a Model Plane Canopy. Part I: The Turbulence Structure. *Boundary-Layer Meteorol.*, 35, 21–52.

7. Yee, E., Kiel, D. and Hilderman, T. (2001). Statistical Characteristics of Plume Dispersion from a Localized Source Within an Obstacle Array in a Water Channel. *Fifth GMU Transport and Dispersion Modelling Workshop*, George Mason University, Fairfax, VA.

8. Belcher, S. E., Jerram, N. and Hunt, J. C. R. (2003). Adjustment of a Turbulent Boundary Layer to a Canopy of Roughness Elements. *J. Fluid Mech.*, 488, 369–398.

9. Hookham, P. A., Lim, D. A. and Hodge, J. K. (2001). Urban Windfield Module. *Fifth GMU Transport and Dispersion Modelling Workshop*, George Mason University, Fairfax, VA.

10. Inouye, E. (1963). On the Turbulent Structure of Airflow Within Crop Canopies. *J. Meteorol. Soc. (Jpn)*, 41, 317–326.

11. Uchijima, Z. and Wright, J. L. (1964). An Experimental Study of Air Flow in a Corn Plant-Air Layer. *Bull. Natl. Inst. Agric. Sci. (Jpn), Ser. A*, 11, 19–65.

12. Cowan, I. R. (1968). Mass, Heat, and Momentum Exchange Between Stands of Plants and Their Atmospheric Environment. *Q. J. R. Meteorol. Soc.*, 94, 318–332.

13. Wilson, N. R. and Shaw, R. H. (1977). A Higher-Order Closure Model for Canopy Flow. *J. Applied Meteorol.*, 16, 1197–1205.

14. Raupach, M. R. and Shaw, R. H. (1982). Averaging Procedures for Flow Within Vegetation Canopies. *Boundary-Layer Meteorol.*, 22, 79–90.

15. Finnigan, J.J. (1985). Turbulent Transport in Flexible Plant Canopies. In B.A. Hutchison

and B.B. Hicks (Eds), *The Forest-Atmosphere Interaction*, pp. 443–480. Boston, MA, D. Reidel Publishing Company.

16. Hanjalic, K., Launder, B. E. and Schiestel, R. (1980). Multiple Time-Scale Concepts in Turbulent Transport Modelling. In L. J. S. Bradbury, F. Durst, B. E. Launder, F. W. Schmidt and J. H. Whitelaw (Eds), *Turbulent Shear Flows*, Vol.II, pp. 36-49. Berlin, Springer-Verlag.

17. Shaw, R. H. and Seginer, I. (1985). The Dissipation of Turbulence in Plant Canopies. *7th A.M.S. Symposium on Turbulence and Diffusion*, Boulder, CO, 200–203.

18. Wilson, J. D. (1988). A Second-Order Closure Model for Flow Through Vegetation. *Boundary-Layer Meteorol.*, 42, 371–392.

19. Schiestel, R. (1987). Multiple-Time-Scale Modelling of Turbulent Flows in One Point Closures. *Phys. Fluids*, 30, 722–731.

20. Wilson, J. D. (1985). Numerical Studies of Flow Through a Windbreak. *J. Wind Eng. Ind. Aerodyn.*, 21, 119–154.

21. Green, S. R. (1992). Modelling Turbulent Air Flow in a Stand of Widely-Spaced Trees. *J. Comp. Fluid Dyn. and Applic.*, 5, 294–312.

22. Wang, H. and Takle, E. S. (1995). Boundary-Layer Flow and Turbulence Near Porous Obstacles: I. Derivation of a General Equation Set For a Porous Media. *Boundary-Layer Meteorol.*, 74, 73–88.

23. Wang, H. and Takle, E.S. (1995). A Numerical Simulation of Boundary-Layer Flows Near Shelterbelts. *Boundary-Layer Meteorol.*, 75, 141–173.

24. Liu, J., Chen, J. M., Black, T. A. and Novak, M. D. (1996). E-ϵ Modelling of Turbulent Air Flow Downwind of a Model Forest Edge. *Boundary-Layer Meteorol.*, 77, 21–44.

25. Ayotte, K. W., Finnigan, J. J. and Raupach, M. R. (1999). A Second-Order Closure for Neutrally Stratified Vegetative Canopy Flows. *Boundary-Layer Meteorol.*, 90, 189–216.

26. Sanz, C. (2003). A Note on k-ϵ Modelling of Vegetation Canopy Air-Flows. *Boundary-Layer Meteorol.*, 108, 191–197.

27. Wilson, J. D. and Yee, E. (2003). Calculation of Winds Disturbed by an Array of Fences. *Agric. For. Meteorol.*, 115, 31–50.

28. Brown, M. J., Lawson, R. E., DeCroix, D. S. and Lee, R. L. (2001). Comparison of Centerline Velocity Measurements Obtained Around 2D and 3D Building Arrays in a Wind Tunnel. (LA-UR-01-4138). Los Alamos National Laboratory.

29. Wilson, J. D. and Mooney, C. J. (1997). Comments on 'A Numerical Simulation of Boundary-Layer Flows Near Shelter Belts' by H. Wang and E. Takle. *Boundary-Layer Meteorol.*, 85, 137–149.

30. Wilson, J. D., Finnigan, J. J. and Raupach, M. R. (1998). A First-Order Closure for Disturbed Plant-Canopy Flows, and its Application to Winds in a Canopy on a Ridge. *Q. J. R. Meteorol. Soc.*, 124, 705–732.

31. Howes, F. A. and Whitaker, S. (1985). The Spatial Averaging Theorem Revisited. *Chem. Eng. Sci.*, 40, 1387–1392.

32. Miguel, A. F., van de Braak, N. J., Silvia, A. M. and Bot, G. P. A. (2001). Wind-Induced

Airflow Through Permeable Materials. Part 1: The Motion Equation. *J. Wind Eng. Indust. Aero.*, 89, 45–57.

33. Getachew, D., Minkowycz, W. J. and Lage, J. L. (2000). A Modified Form of the k-ϵ Model for Turbulent Flows of an Incompressible Fluid in Porous Media. *Int. J. Heat Mass Transfer*, 43, 2909–2915.

34. Launder, B. E. and Spalding, D. B. (1974). The Numerical Computation of Turbulent Flows. *Comp. Methods Appl. Mech. Eng.*, 3, 269–289.

35. Daly, B. J. and Harlow, F. H. (1970). Transport Equations of Turbulence. *Phys. Fluids*, 13, 2634–2649.

36. Ince, N. Z. and Launder, B. E. (1989). On the Computation of Buoyancy-Driven Turbulent Flows in Rectangular Enclosures. *Int. J. Heat Mass Transfer*, 10, 110–117.

37. Durbin, P. A. and Pettersson Reif, B. A. (2001). *Statistical Theory and Modelling for Turbulent Flows*, John Wiley & Sons, New York.

38. Raupach, M. R. and Thom, A. S. (1981). Turbulence In and Above Plant Canopies. *Ann. Rev. Fluid Mech.*, 13, 97–129.

39. Lee, K. and Howell, J. R. (1987). Forced Convective and Radiative Transfer Within a Highly Porous Layer Exposed to a Turbulent External Flow Field. *Proc. ASME-JSME Thermal Engineering Joint Conference*, Washington, D.C., USA.

40. Raupach, M. R., Finnigan, J. J. and Brunet, Y. (1996). Coherent Eddies and Turbulence in Vegetation Canopies: The Mixing Layer Analogy. *Boundary-Layer Meteorol.*, 78, 351–382.

41. Launder, B. E., Reece, G. J. and Rodi, W. (1975). Progress in the Development of a Reynolds Stress Turbulence Closure. *J. Fluid Mech.*, 68, 537–566.

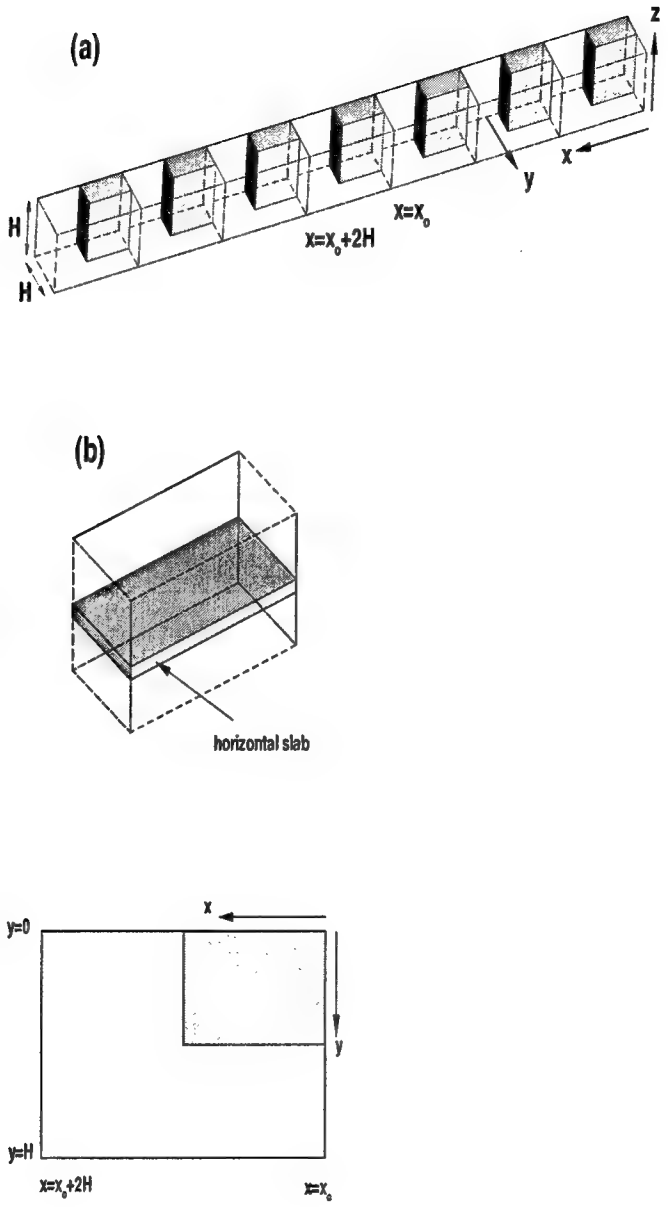

Figure 1. Decomposition of the aligned array of cubes into (a) seven drag units with each drag unit consisting of a row of cubes and the associated downstream canyon; (b) thin horizontal slab chosen as the averaging volume within each drag unit.

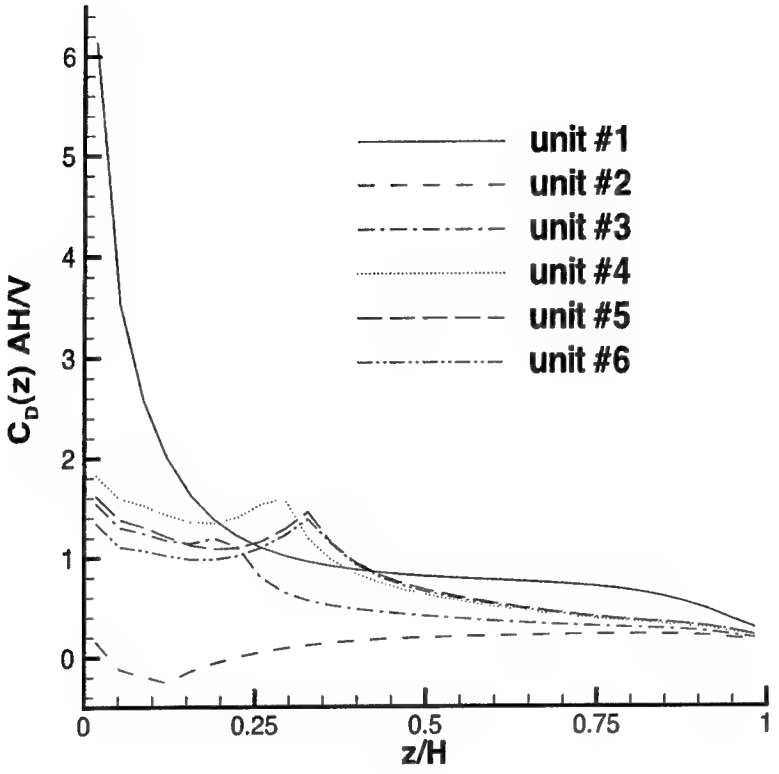

Figure 2. The variation of normalized sectional (local) drag coefficient $C_D(z)AH/V \equiv C_D(z)\hat{A}$ for each drag unit comprising the building array.

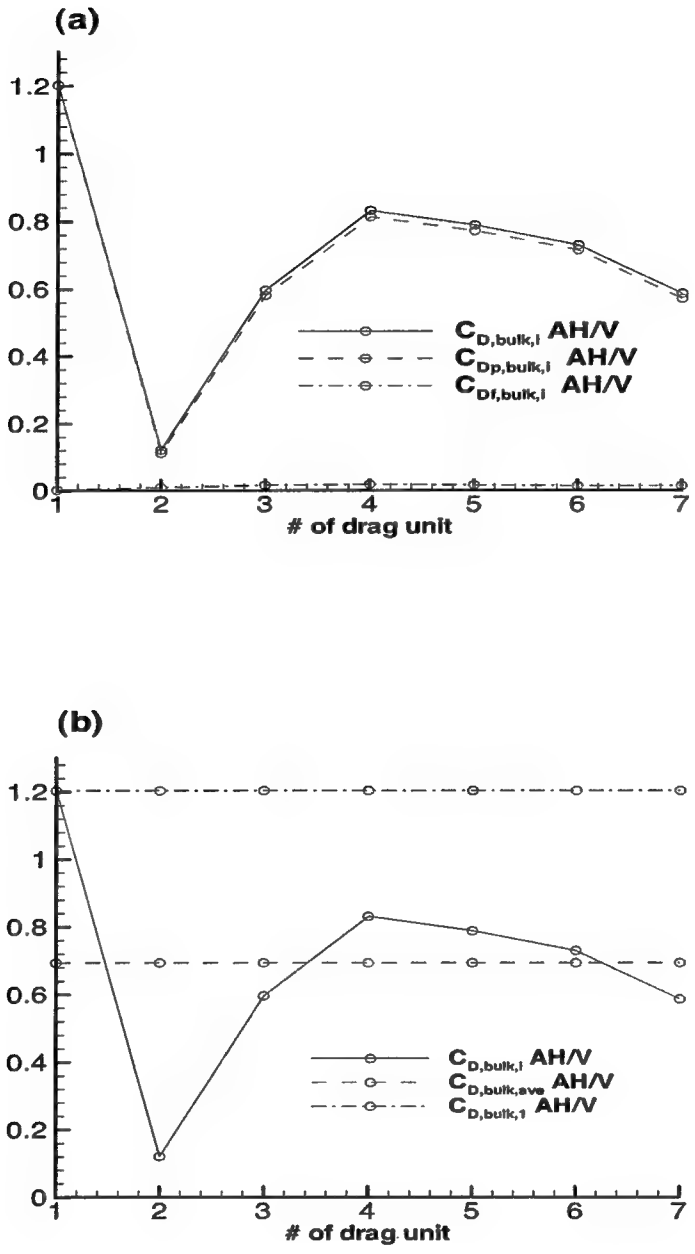

Figure 3. The normalized bulk drag coefficients for various drag units in the building array: (a) $C_{D,\text{bulk},i}AH/V$, $C_{Dp,\text{bulk},i}AH/V$ and $C_{Df,\text{bulk},i}AH/V$; (b) $C_{D,\text{bulk},i}AH/V$, $C_{D,\text{bulk,ave}}AH/V$, and $C_{D,\text{bulk},1}AH/V$.

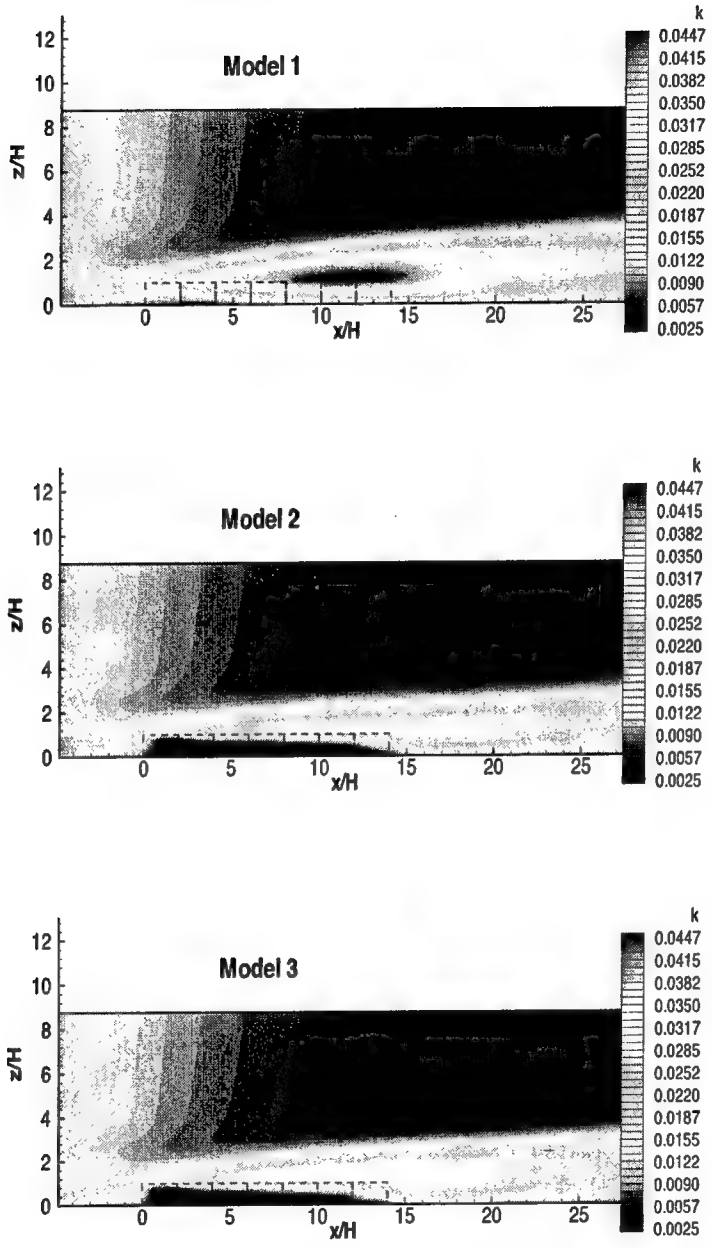

Figure 4. Turbulence kinetic energy ($\overline{\kappa}$) isopleths obtained with three different k-ϵ closure models used in conjunction with the diagnosed values for the sectional (local) drag coefficient $C_D(z)$.

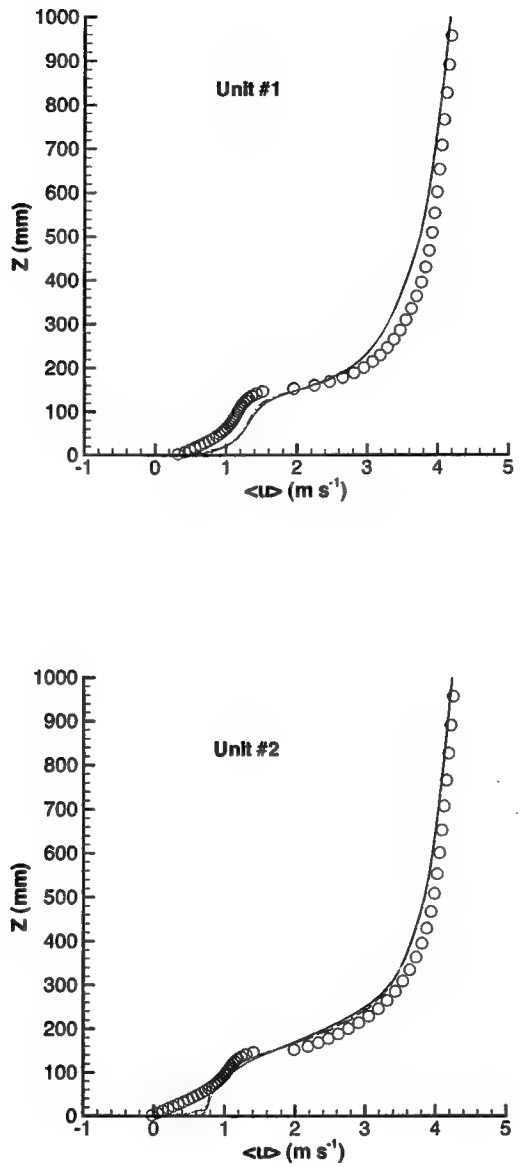

Figure 5. Profiles of $\langle \tilde{u} \rangle$ obtained with three different k-ϵ closure models used in conjunction with the diagnosed values for the sectional (local) drag coefficient $C_D(z)$ for drag units #1 and #2. Model 1 (solid line); Model 2 (dashed line); Model 3 (dashed-dotted line); high-resolution CFD (open circle).

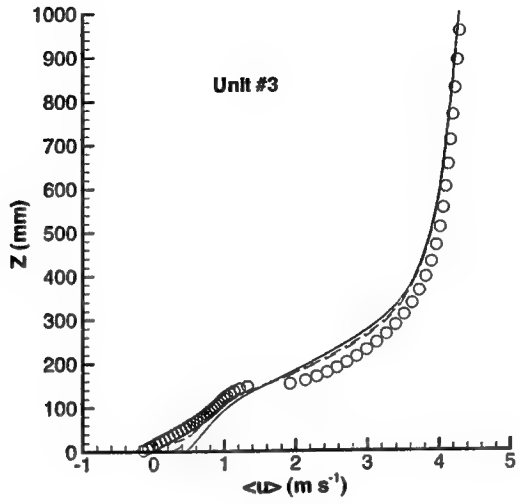

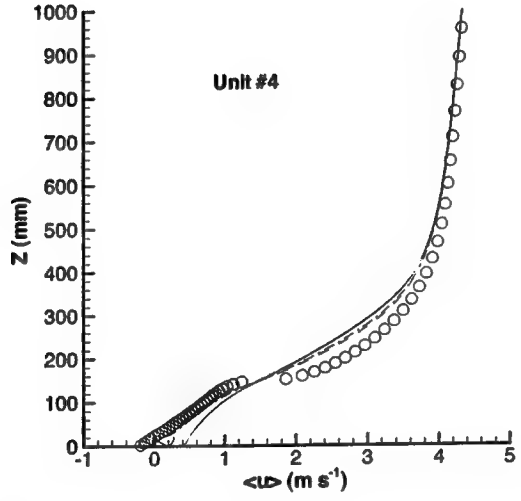

Figure 5. (Continued) Profiles of $\langle \bar{u} \rangle$ obtained with three different k-ϵ closure models used in conjunction with the diagnosed values for the sectional (local) drag coefficient $C_D(z)$ for drag units #3 and #4. Model 1 (solid line); Model 2 (dashed line); Model 3 (dashed-dotted line); high-resolution CFD (open circle).

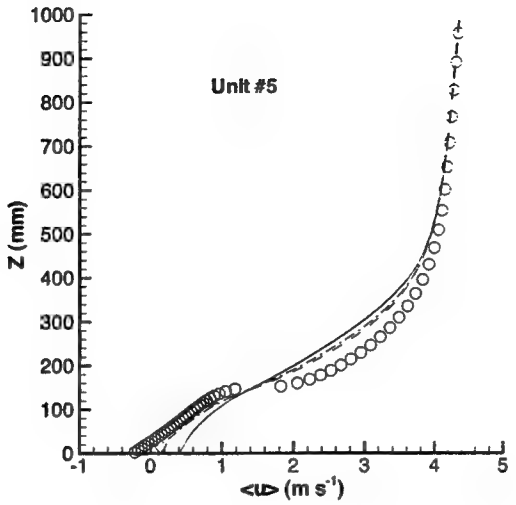

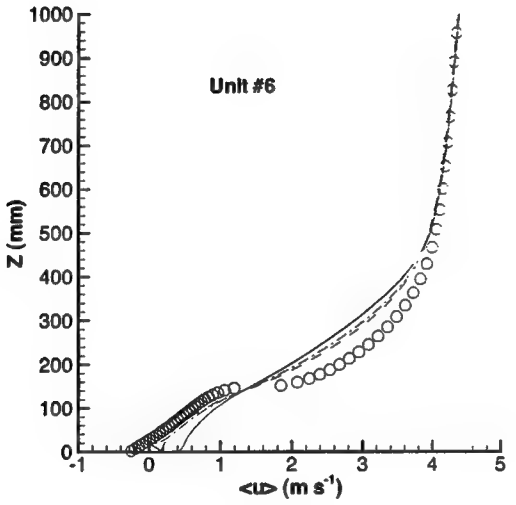

Figure 5. (Continued) Profiles of $\langle \bar{u} \rangle$ obtained with three different k-ϵ closure models used in conjunction with the diagnosed values for the sectional (local) drag coefficient $C_D(z)$ for drag units #5 and #6. Model 1 (solid line); Model 2 (dashed line); Model 3 (dashed-dotted line); high-resolution CFD (open circle).

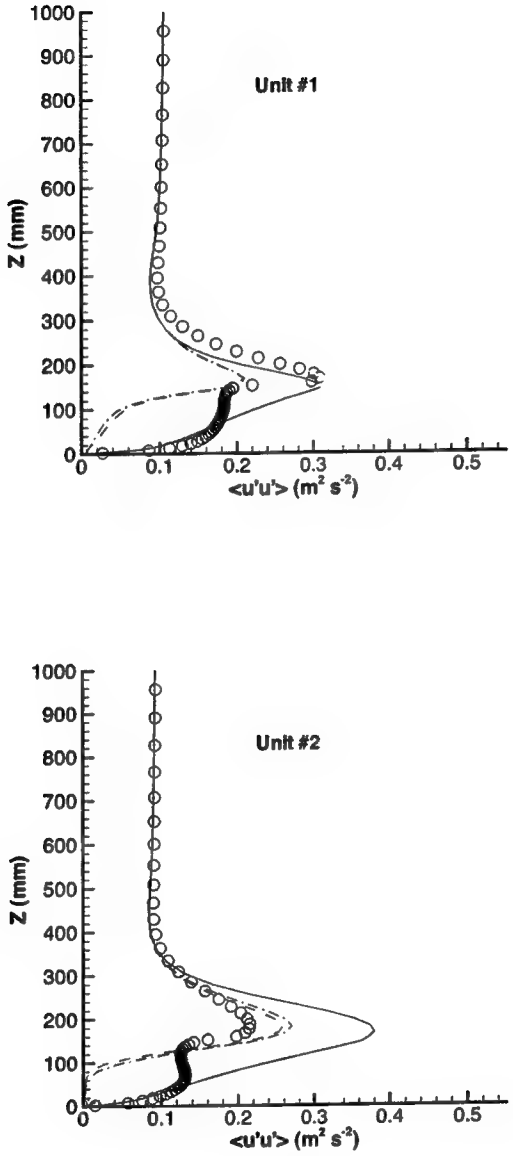

Figure 6. Profiles of $\overline{\langle u' \rangle \langle u' \rangle}$ obtained with three different k-ϵ closure models used in conjunction with the diagnosed values for the sectional (local) drag coefficient $C_D(z)$ for drag units #1 and #2. Model 1 (solid line); Model 2 (dashed line); Model 3 (dashed-dotted line); high-resolution CFD (open circle).

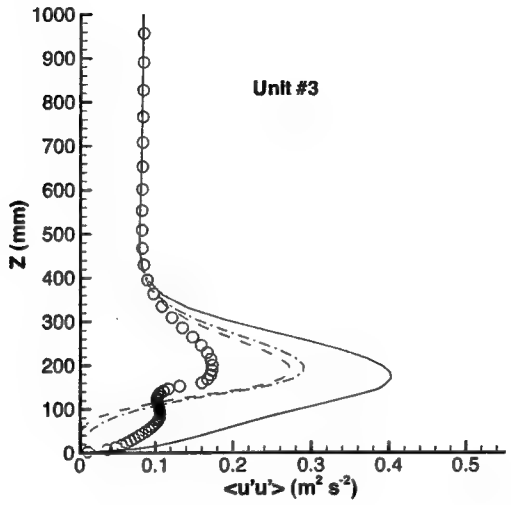

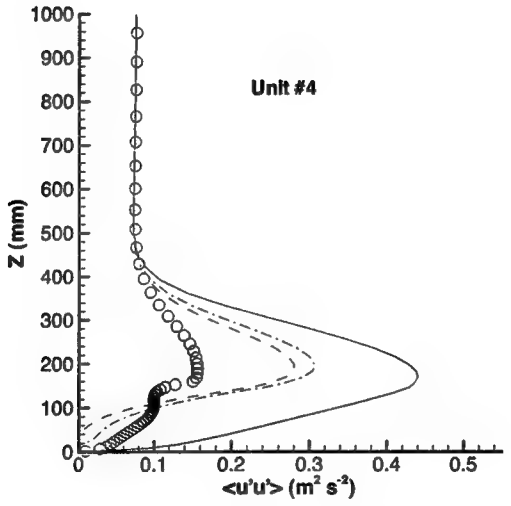

Figure 6. (Continued) Profiles of $\overline{\langle u' \rangle \langle u' \rangle}$ obtained with three different k-ϵ closure models used in conjunction with the diagnosed values for the sectional (local) drag coefficient $C_D(z)$ for drag units #3 and #4. Model 1 (solid line); Model 2 (dashed line); Model 3 (dashed-dotted line); high-resolution CFD (open circle).

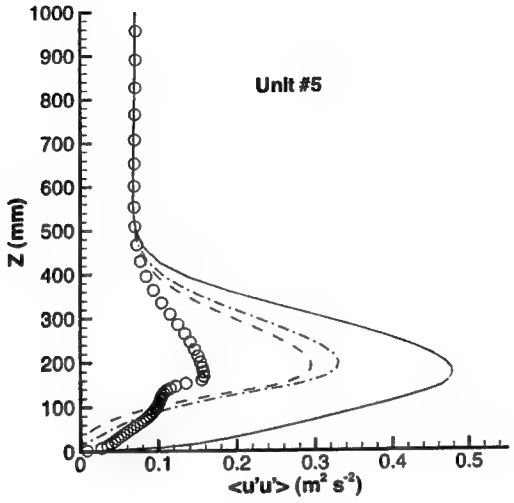

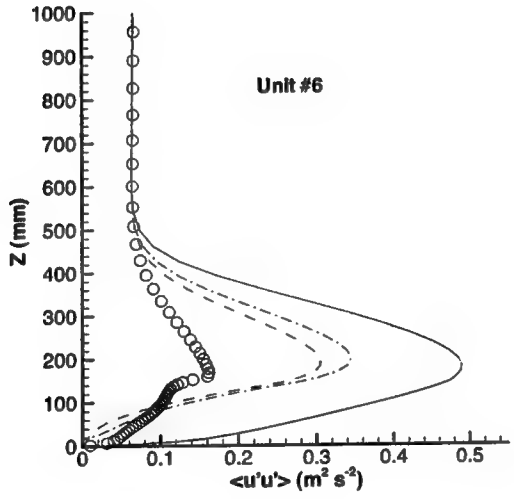

Figure 6. (Continued) Profiles of $\overline{\langle u' \rangle \langle u' \rangle}$ obtained with three different k-ϵ closure models used in conjunction with the diagnosed values for the sectional (local) drag coefficient $C_D(z)$ for drag units #5 and #6. Model 1 (solid line); Model 2 (dashed line); Model 3 (dashed-dotted line): high-resolution CFD (open circle).

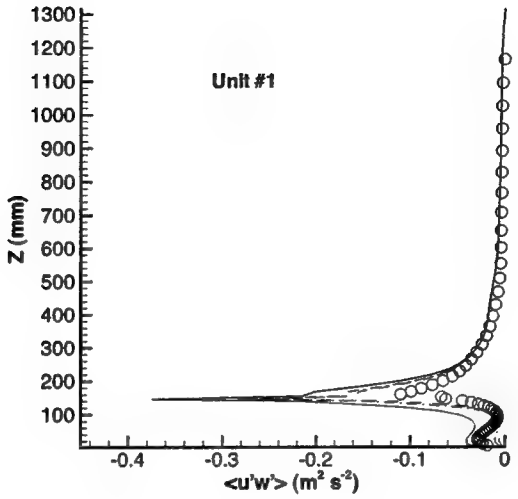

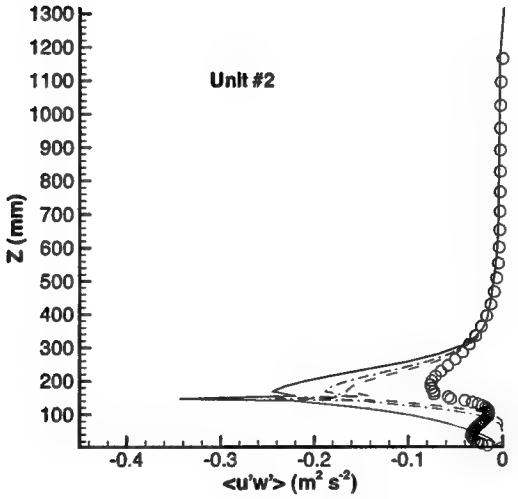

Figure 7. Profiles of $\overline{\langle u' \rangle \langle w' \rangle}$ obtained with three different k-ϵ closure models used in conjunction with the diagnosed values for the sectional (local) drag coefficient $C_D(z)$ for drag units #1 and #2. Model 1 (solid line); Model 2 (dashed line); Model 3 (dashed-dotted line); high-resolution CFD (open circle).

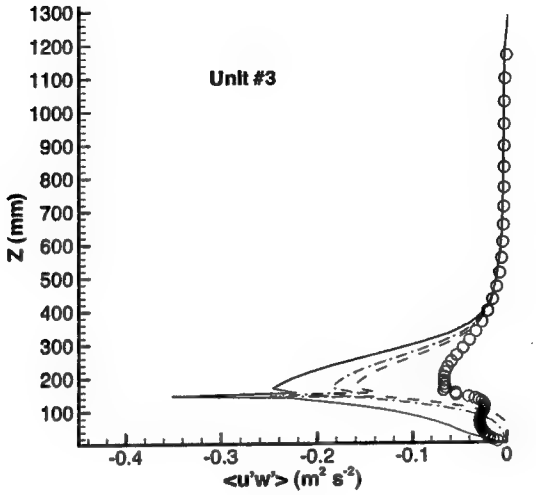

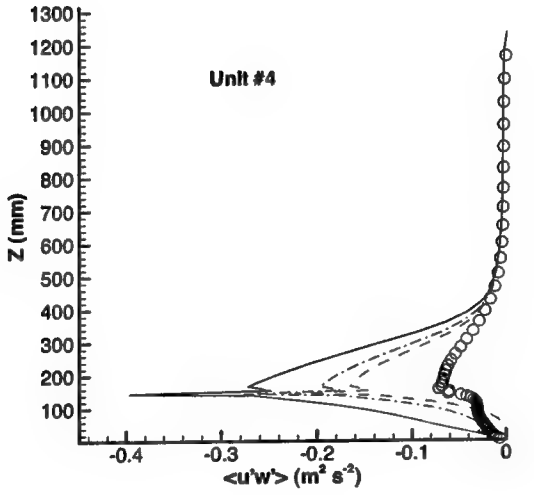

Figure 7. (Continued) Profiles of $\overline{\langle u' \rangle \langle w' \rangle}$ obtained with three different k-ϵ closure models used in conjunction with the diagnosed values for the sectional (local) drag coefficient $C_D(z)$ for drag units #3 and #4. Model 1 (solid line); Model 2 (dashed line); Model 3 (dashed-dotted line); high-resolution CFD (open circle).

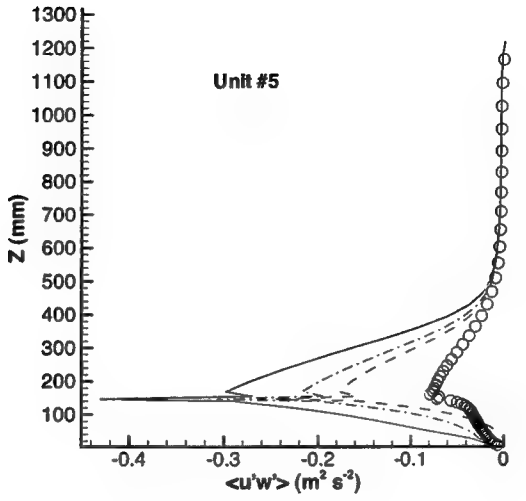

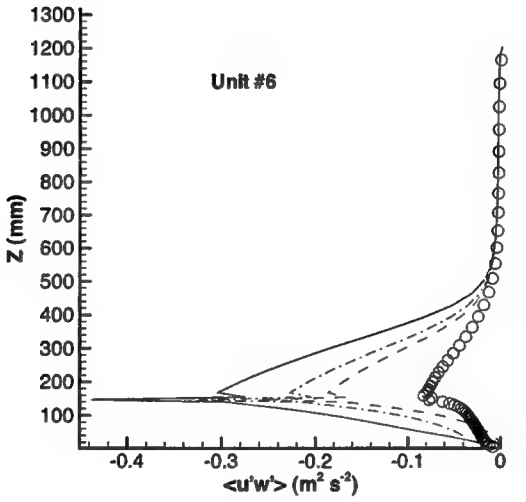

Figure 7. (Continued) Profiles of $\overline{\langle u' \rangle \langle w' \rangle}$ obtained with three different k-ϵ closure models used in conjunction with the diagnosed values for the sectional (local) drag coefficient $C_D(z)$ for drag units #5 and #6. Model 1 (solid line): Model 2 (dashed line); Model 3 (dashed-dotted line); high-resolution CFD (open circle).

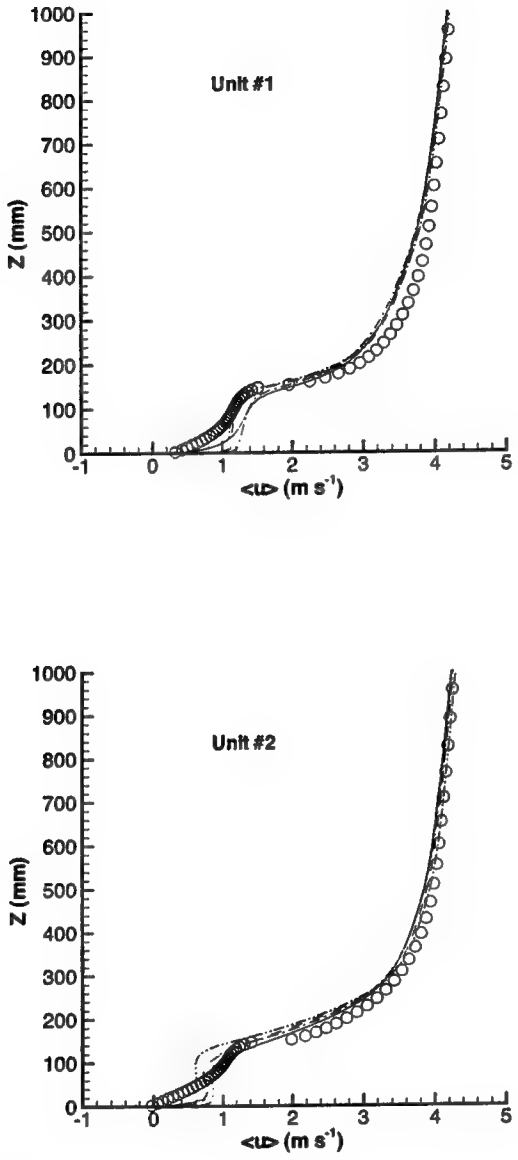

Figure 8. Profiles of $\langle \bar{u} \rangle$ obtained with the proposed distributed drag force model (Model 3) used in conjunction with four different methods for specifying the drag coefficient. $C_D(z)$ (solid line); $C_{D,\text{bulk},i}$ (dashed line); $C_{D,\text{bulk,ave}}$ (dashed-dotted line); $C_{D,\text{bulk},1}$ (dashed-dotted-dotted line); high-resolution CFD (open circle). Results are shown for drag units #1 and #2.

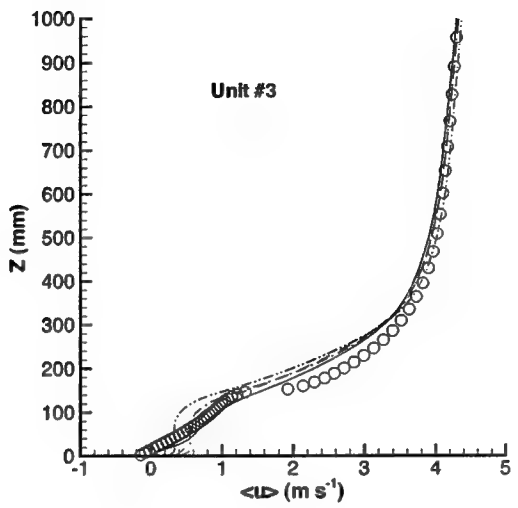

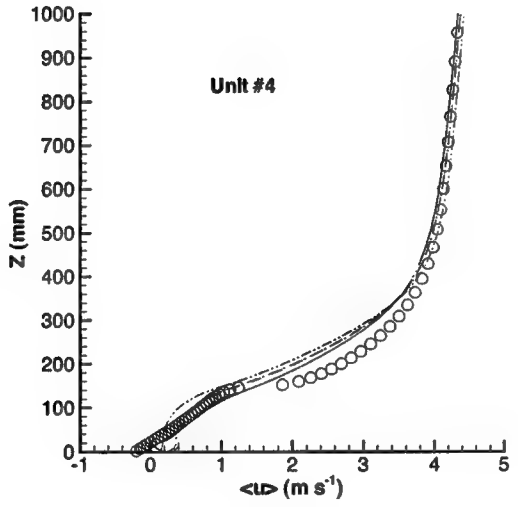

Figure 8. (Continued) Profiles of $\langle \bar{u} \rangle$ obtained with the proposed distributed drag force model (Model 3) used in conjunction with four different methods for specifying the drag coefficient. $C_D(z)$ (solid line); $C_{D,\text{bulk},i}$ (dashed line); $C_{D,\text{bulk,ave}}$ (dashed-dotted line); $C_{D,\text{bulk},1}$ (dashed-dotted-dotted line); high-resolution CFD (open circle). Results are shown for drag units #3 and #4.

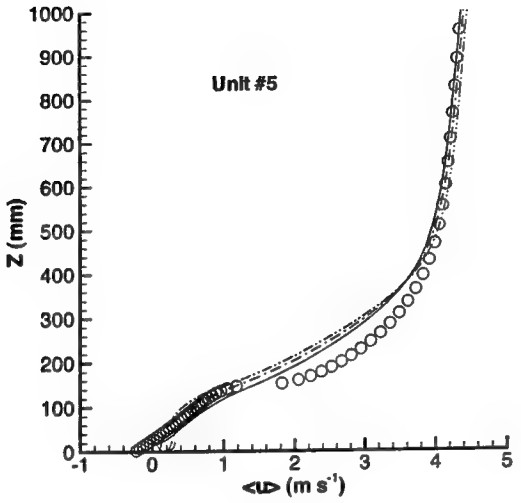

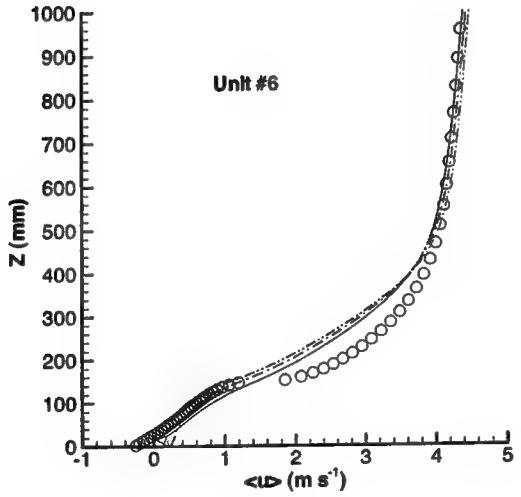

Figure 8. (Continued) Profiles of $\langle \bar{u} \rangle$ obtained with the proposed distributed drag force model (Model 3) used in conjunction with four different methods for specifying the drag coefficient. $C_D(z)$ (solid line); $C_{D,\text{bulk},i}$ (dashed line); $C_{D,\text{bulk,ave}}$ (dashed-dotted line); $C_{D.\text{bulk.1}}$ (dashed-dotted-dotted line); high-resolution CFD (open circle). Results are shown for drag units #5 and #6.

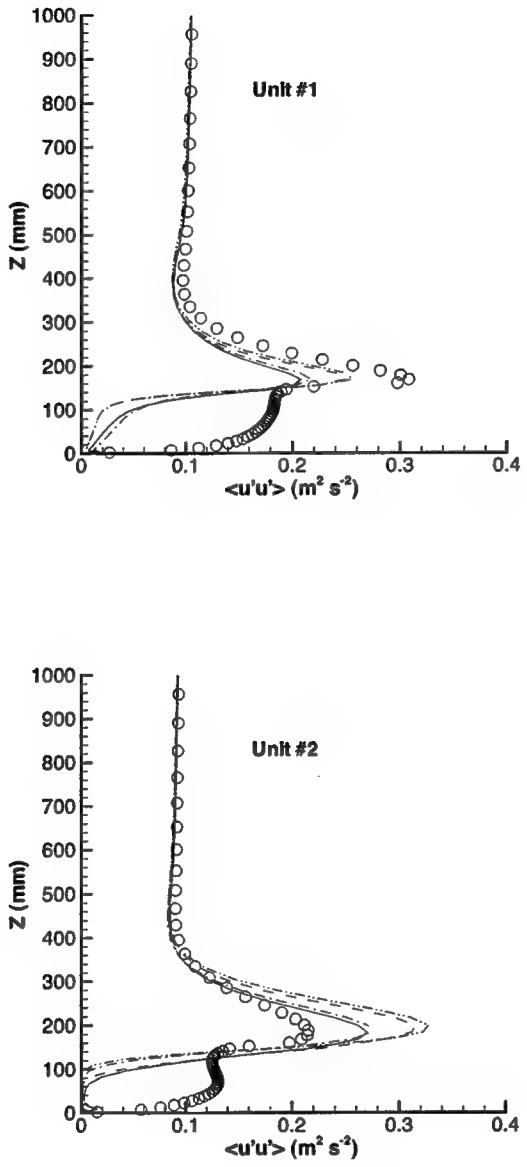

Figure 9. Profiles of $\overline{\langle u' \rangle \langle u' \rangle}$ obtained with the proposed distributed drag force model (Model 3) used in conjunction with four different methods for specifying the drag coefficient. $C_D(z)$ (solid line); $C_{D,\text{bulk},i}$ (dashed line); $C_{D,\text{bulk,ave}}$ (dashed-dotted line); $C_{D,\text{bulk},1}$ (dashed-dotted-dotted line); high-resolution CFD (open circle). Results are shown for drag units #1 and #2.

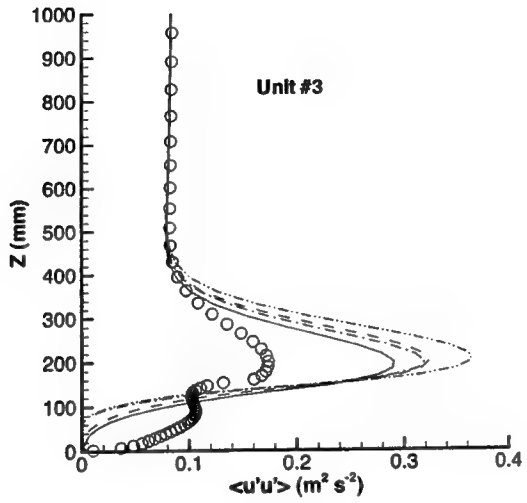

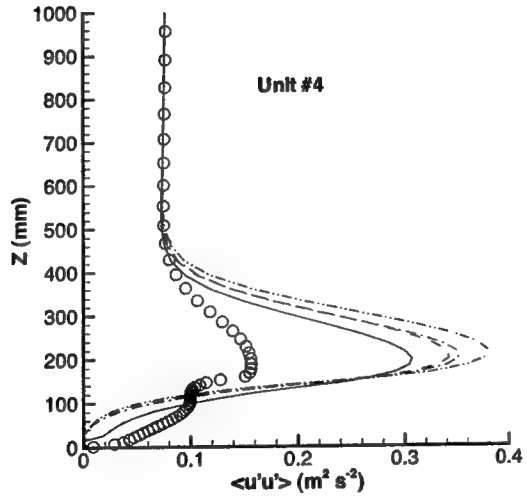

Figure 9. (Continued) Profiles of $\overline{\langle u' \rangle \langle u' \rangle}$ obtained with the proposed distributed drag force model (Model 3) used in conjunction with four different methods for specifying the drag coefficient. $C_D(z)$ (solid line); $C_{D,\text{bulk},i}$ (dashed line); $C_{D,\text{bulk,ave}}$ (dashed-dotted line); $C_{D,\text{bulk},1}$ (dashed-dotted-dotted line); high-resolution CFD (open circle). Results are shown for drag units #3 and #4.

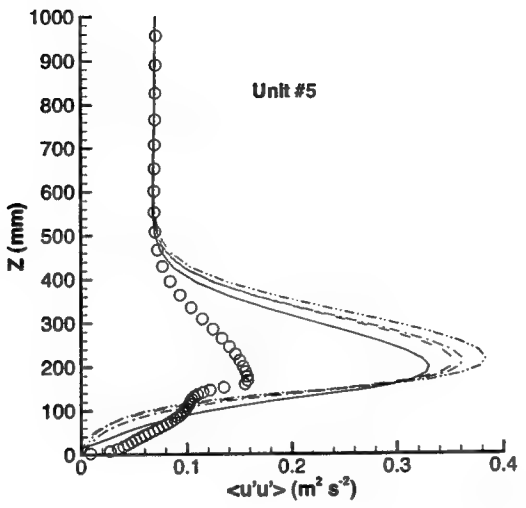

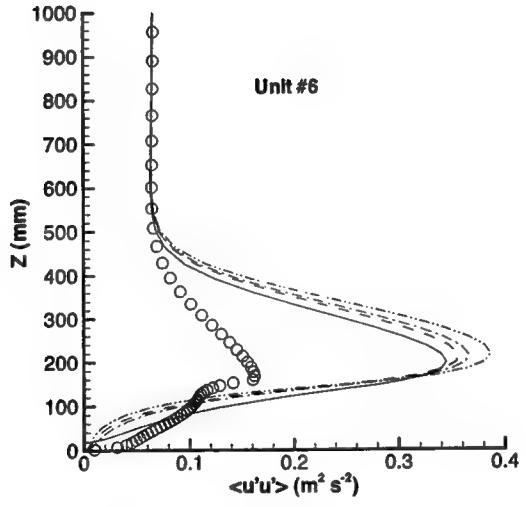

Figure 9. (Continued) Profiles of $\overline{\langle u' \rangle \langle u' \rangle}$ obtained with the proposed distributed drag force model (Model 3) used in conjunction with four different methods for specifying the drag coefficient. $C_D(z)$ (solid line); $C_{D,\text{bulk},\tilde{t}}$ (dashed line); $C_{D,\text{bulk,ave}}$ (dashed-dotted line); $C_{D,\text{bulk},1}$ (dashed-dotted-dotted line); high-resolution CFD (open circle). Results are shown for drag units #5 and #6.

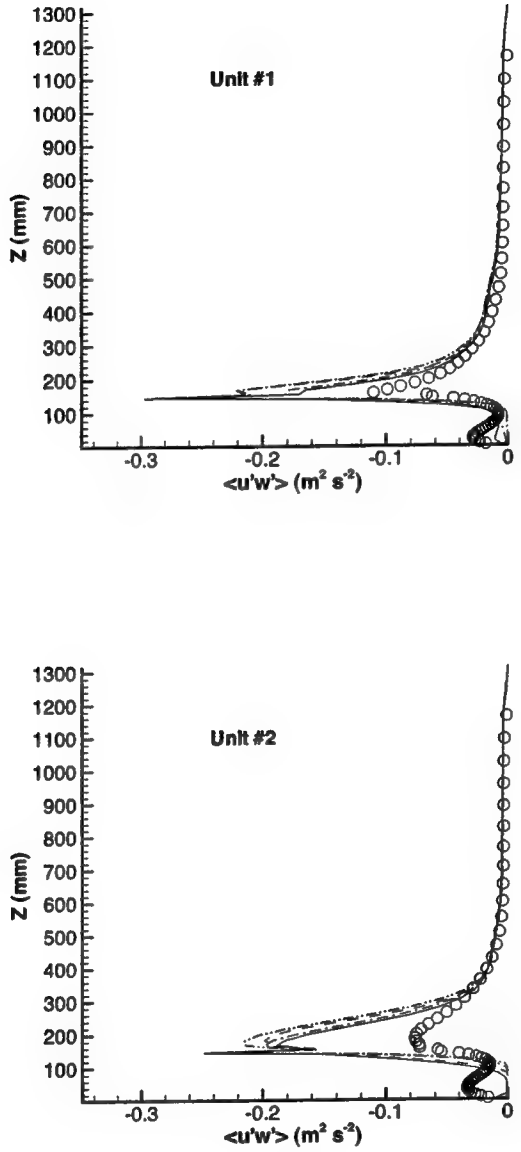

Figure 10. Profiles of $\overline{\langle u' \rangle \langle w' \rangle}$ obtained with the proposed distributed drag force model (Model 3) used in conjunction with four different methods for specifying the drag coefficient. $C_D(z)$ (solid line); $C_{D,\text{bulk},i}$ (dashed line); $C_{D,\text{bulk,ave}}$ (dashed-dotted line); $C_{D,\text{bulk},1}$ (dashed-dotted-dotted line); high-resolution CFD (open circle). Results are shown for drag units #1 and #2.

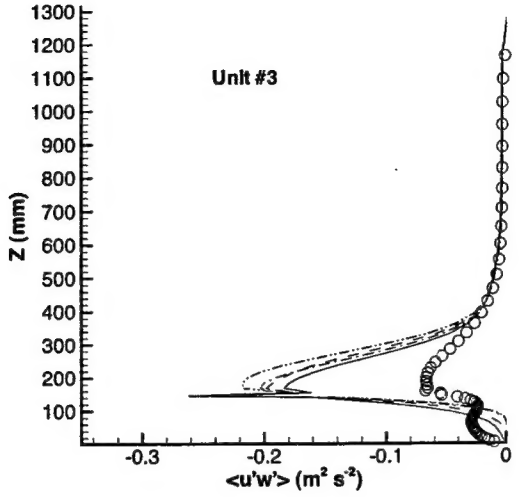

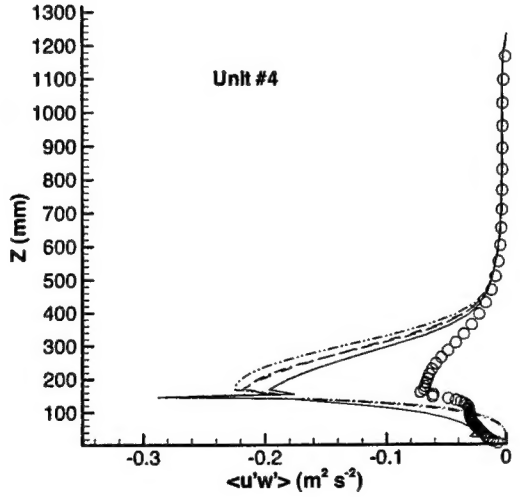

Figure 10. (Continued) Profiles of $\overline{\langle u' \rangle \langle w' \rangle}$ obtained with the proposed distributed drag force model (Model 3) used in conjunction with four different methods for specifying the drag coefficient. $C_D(z)$ (solid line); $C_{D,\text{bulk},i}$ (dashed line); $C_{D,\text{bulk,ave}}$ (dashed-dotted line); $C_{D,\text{bulk},1}$ (dashed-dotted-dotted line); high-resolution CFD (open circle). Results are shown for drag units #3 and #4.

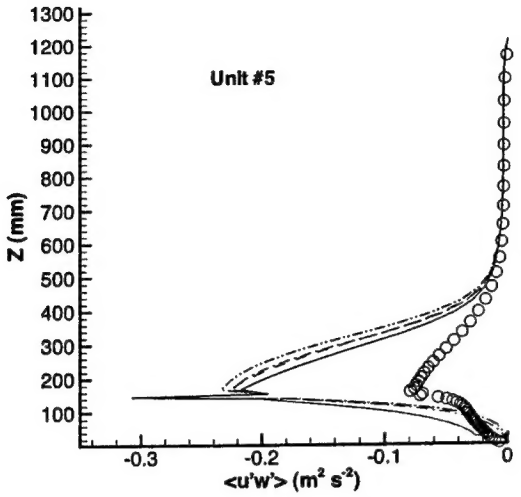

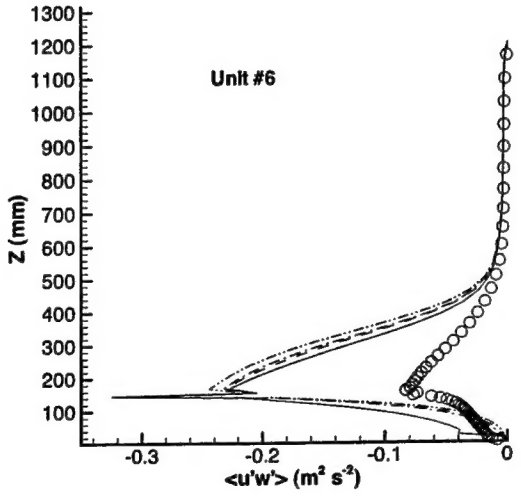

Figure 10. (Continued) Profiles of $\overline{\langle u' \rangle \langle w' \rangle}$ obtained with the proposed distributed drag force model (Model 3) used in conjunction with four different methods for specifying the drag coefficient. $C_D(z)$ (solid line); $C_{D,\text{bulk},i}$ (dashed line); $C_{D,\text{bulk,ave}}$ (dashed-dotted line); $C_{D,\text{bulk},1}$ (dashed-dotted-dotted line); high-resolution CFD (open circle). Results are shown for drag units #5 and #6.

UNCLASSIFIED

SECURITY CLASSIFICATION OF FORM

(highest classification of Title, Abstract, Keywords)

DOCUMENT CONTROL DATA

(Security classification of title, body of abstract and indexing annotation must be entered when the overall document is classified)

1. ORIGINATOR (the name and address of the organization preparing the document. Organizations for who the document was prepared, e.g. Establishment sponsoring a contractor's report, or tasking agency, are entered in Section 8.)

   Defence R&D Canada – Suffield
   PO Box 4000, Station Main
   Medicine Hat, AB T1A 8K6

2. SECURITY CLASSIFICATION (overall security classification of the document, including special warning terms if applicable)

   Unclassified

3. TITLE (the complete document title as indicated on the title page. Its classification should be indicated by the appropriate abbreviation (S, C or U) in parentheses after the title).

   A Distributed Drag Force Approach for the Numerical Simulation of Urban Flows (U)

4. AUTHORS (Last name, first name, middle initial. If military, show rank, e.g. Doe, Maj. John E.)

   Yee, E. and Lien, F.S.

5. DATE OF PUBLICATION (month and year of publication of document)

   November 2004

6a. NO. OF PAGES (total containing information, include Annexes, Appendices, etc) 58

6b. NO. OF REFS (total cited in document) 41

7. DESCRIPTIVE NOTES (the category of the document, e.g. technical report, technical note or memorandum. If appropriate, enter the type of report, e.g. interim, progress, summary, annual or final. Give the inclusive dates when a specific reporting period is covered.)

   Technical Report

8. SPONSORING ACTIVITY (the name of the department project office or laboratory sponsoring the research and development. Include the address.)

   Defence R&D Canada – Suffield

9a. PROJECT OR GRANT NO. (If appropriate, the applicable research and development project or grant number under which the document was written. Please specify whether project or grant.)

   16QD40

9b. CONTRACT NO. (If appropriate, the applicable number under which the document was written.)

10a. ORIGINATOR'S DOCUMENT NUMBER (the official document number by which the document is identified by the originating activity. This number must be unique to this document.)

   DRDC Suffield TR 2004-169

10b. OTHER DOCUMENT NOs. (Any other numbers which may be assigned this document either by the originator or by the sponsor.)

11. DOCUMENT AVAILABILITY (any limitations on further dissemination of the document, other than those imposed by security classification)

   (x) Unlimited distribution
   ( ) Distribution limited to defence departments and defence contractors; further distribution only as approved
   ( ) Distribution limited to defence departments and Canadian defence contractors; further distribution only as approved
   ( ) Distribution limited to government departments and agencies; further distribution only as approved
   ( ) Distribution limited to defence departments; further distribution only as approved
   ( ) Other (please specify):

12. DOCUMENT ANNOUNCEMENT (any limitation to the bibliographic announcement of this document. This will normally corresponded to the Document Availability (11). However, where further distribution (beyond the audience specified in 11) is possible, a wider announcement audience may be selected).

   Unlimited

13. ABSTRACT (a brief and factual summary of the document. It may also appear elsewhere in the body of the document itself. It is highly desirable that the abstract of classified documents be unclassified. Each paragraph of the abstract shall begin with an indication of the security classification of the information in the paragraph (unless the document itself is unclassified) represented as (S), (C) or (U). It is not necessary to include here abstracts in both official languages unless the text is bilingual).

A modified k-ε model is proposed for the simulation of the mean wind speed and turbulence for a neutrally-stratified flow through and over a building array, where groups of buildings in the array are aggregated and treated as a porous barrier. This model is based on time averaging the spatially-averaged Navier-Stokes equation, in which the effects of the obstacle-atmosphere interaction are included through the introduction of a volumetric momentum sink (representing drag on the unresolved buildings in the array). In addition, closure of the time-averaged, spatially-averaged Navier-Stokes equations requires two additional prognostic equations, namely one for the time-averaged sub-filter kinetic energy, $\overline{\kappa}$, and another for the dissipation rate, ε, of $\overline{\kappa}$. The transport equation for $\overline{\kappa}$ can be derived from first principles and explicitly includes additional sources and sinks that arise from time averaging the product of the spatially-averaged velocity fluctuations and the distributed drag force fluctuations. The latter time-averaged product can be approximated systematically to any degree of accuracy using a Taylor series expansion and, to this end, a high-order approximation is derived to represent this source/sink term in the transport equation for $\overline{\kappa}$ which corresponds physically to the work done against pressure (form) and viscous drag in the building array. The dissipation rate (ε-) equation is simply obtained as a dimensionally consistent analog of the $\overline{\kappa}$-equation.

Because measurements of the spatially-averaged velocity statistics in obstacle arrays are not available, the performance of the proposed model and some simplified versions derived from it are compared with the spatially-averaged, time-mean velocity and various spatially-averaged Reynolds stresses diagnosed from high-resolution computational fluid dynamics (CFD) simulations of the flow within and over an aligned array of sharp-edged cubes with a plan area density of 0.25. However, it should be emphasized that the high-resolution CFD flow simulations have been validated with wind tunnel experiments, and after these validations the model can be used to diagnose the spatially-averaged velocity statistics required for the validation of the distributed drag force model. It was found that the model predictions for mean wind speed and turbulence in the building array were not sensitive to the differing treatments of the source and sink terms in the $\overline{\kappa}$- and ε-equations, implying that the high-order approximations of these source/sink terms did not offer any predictive advantage. A possible explanation for this is the utilization of the Boussinesq linear stress-strain constitutive relation within the k-ε modelling framework, whose implicit omission of any anisotropic eddy-viscosity effects renders it incapable of predicting any strong anisotropy of the turbulence field that might exist in the building array. Four different methods for diagnosis of the drag coefficient C_D for the aligned cube array, required for the volumetric drag force representation of the cubes, are investigated here.

14. KEYWORDS, DESCRIPTORS or IDENTIFIERS (technically meaningful terms or short phrases that characterize a document and could be helpful in cataloguing the document. They should be selected so that no security classification is required. Identifies, such as equipment model designation, trade name, military project code name, geographic location may also be included. If possible keywords should be selected from a published thesaurus, e.g. Thesaurus of Engineering and Scientific Terms (TEST) and that thesaurus-identified. If it is not possible to select indexing terms which are Unclassified, the classification of each should be indicated as with the title.)

Urban Flow Modeling
Building Arrays
Computational Fluid Dynamics
Distributed Drag Force
Determination of Drag Coefficient
Spatally-averaged velocity statistics